國立臺灣大學電機資訊學院電信工程學研究所

碩士論文

Graduate Institute of Communication Engineering

College of Electrical Engineering ＆ Computer Science

National Taiwan University

Master Thesis

應用於現代無線通訊系統之低溫共燒陶瓷雙工器設計

Low Temperature Co-Fired Ceramic Duplexer Designs for

Modern Wireless Communication System

蔡柏原

Po-Yuan Tsai

指導教授：吳宗霖 博士

Advisor: Tzong-Lin Wu, Ph.D.

中華民國 104 年 6 月

June, 2015

國立臺灣大學碩士學位論文
口試委員會審定書

應用於現代無線通訊系統之低溫共燒陶瓷雙工器設計

Low Temperature Co-Fired Ceramic Duplexer Designs for

Modern Wireless Communication System

本論文係蔡柏原君（R02942004）在國立臺灣大學電信工程學研究所完成之碩士學位論文，於民國 104 年 06 月 26 日承下列考試委員審查通過及口試及格，特此證明

口試委員：

_____（簽名）

（指導教授）

所　　長　_____（簽名）

誌謝

時光荏苒，一晃眼又是一段美好時光的結束。回想兩年生涯，有甘有苦，難以盡述，然而每個精彩片段，都令我回味不已。

有幸加入 EMC Lab 這個充滿人情味的大家庭，得之於人者太多，感謝摯愛的導師吳宗霖教授，老師不只傳授紮實的專業知識，也常與我們分享人生體悟，開導我們心中疑惑，實可謂「傳道、授業、解惑」之良師！同時也感謝口試委員馬自莊教授、盧信嘉教授、王挺光博士及許森貴博士給予的寶貴建議，使本論文能更臻完善。

當初剛入學的自己，對各方面都一知半解，感謝貴人一號麵包帥哥，幫我打好基礎，一步一步地帶著我進入濾波器的世界，學長總是不厭其煩的解答我各種奇怪的問題，在學長研究忙碌之時，也必定不忘照看學弟可憐的進度，至今銘感五內。還記得一年級時為了想研究題目，跟學長常常在電腦面前看著 paper 皺眉沉思，雖然腦袋很痛，但那時我真的體會到研究的樂趣所在。

一下時，遇到了深耕計畫，有幸能接受本實驗室濾波器王者貴人二號揚智帥哥的指導，沒有學長的不時接濟，我可能連起頭都大有困難。學長身懷濾波器深厚素養，在我看來如果早點出生，大概耦合矩陣就是你提出來了。學長除了在深耕給予的強力支援外，平時也是絕佳的聊天對象，本來預計討論 10 分鐘，卻常常變成兩小時......。量測時，也是花費了學長許多時間，想來真是過意不去。

志穎學長及齊軒學長時常會給予我精確的建議，讓我明白可以修正的方向，尤其齊軒學長在大家口試預演時的建議都一針見血，非常受用。求致學長在理論上的造詣之高，總是令我嘆服(雖然常常聽不懂)。英誠學長的單導體雜訊抑制，想必會成為實驗室未來的秘密武器。同屆的振家、文譯及靜慧，我不會忘記與你們在實驗室奮鬥那些超過 12 點的日子。學弟妹晉毅、彥如、亦如、庭毅、毅安，個個實力堅強，未來難以限量，害我都不好意思說我是學長。庭毅，當有一天你喊出 King of RF 的名號，別忘了燒個 Duplexer 給我，我在地下也會笑的。

最後不免俗的感謝我堅實的後盾，我親愛的父母及老哥，有他們的全力支持，我才能心無罣礙的完成學位。

<div align="right">2015.7.31 蔡柏原</div>

中文摘要

　　雙工器是現代無線通訊系統中的關鍵元件，其主要功能為將不同頻率成分的訊號分流至不同路徑。雙工器可使發射機與接收機共用一支天線，因此可省下額外的天線成本。雙工器有許多設計方法，其中一個方法為使用 T 型接面或雙模態共振器做為匹配電路結合兩個帶通濾波器。然而，由於此匹配電路與導波結構中的電氣長度有關，因此往往不利於縮小化設計。另一個方法是使用人造傳輸線產生不同訊號路徑，雖然整體電路面積可大幅縮小，但對隔離度的要求通常需有所取捨。因此，本篇論文將交叉耦合帶通濾波器與微型化匹配電路結合，提出一集總式雙工器電路，可同時達到高隔離度及小尺寸的設計目標。

　　於簡介完交叉耦合帶通濾波器的理論基礎後，本篇論文先提出一個方法補償導抗轉換器的非理想特性。藉由引入更多設計自由度，通帶內的不匹配以及頻率偏移可有效補償，利於設計集總式帶通濾波器。當兩個所需的帶通濾波器設計完畢，便可依據本篇論文理論加入一集總式匹配電路，完成雙工器設計。本篇論文提出的雙工器可達至 50 dB 的隔離度，且電路大小只有 $0.072\lambda_g \times 0.038\lambda_g$，與文獻中的雙工器相比，本論文所提出的電路具有高隔離度並能達到較小的電路尺寸。

　　此外，本論文也提出一個用於兩個緊鄰頻帶的雙工器電路，隔離度可藉由電路中同時存在的高阻抗及低阻抗路徑有所提升，而使用高選擇性帶通濾波器可減低雙工器在 GPS 以及 Bluetooth 頻帶所受的干擾。本論文提出的架構可達至 38 dB 的隔離度，並在 GPS 及 Bluetooth 頻帶提供至少 30 dB 的雜訊抑制。
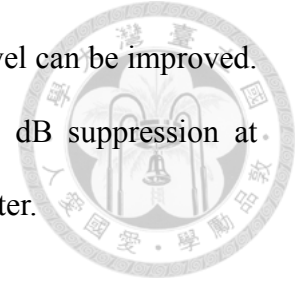
關鍵字：雙工器、匹配電路、隔離度、集總式架構、微型化

ABSTRACT
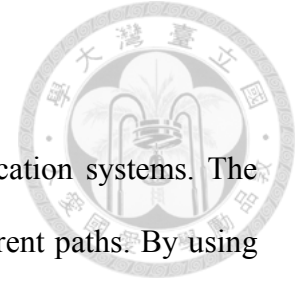
Duplexers are key components in modern wireless communication systems. The main function is dividing signals of different frequencies into different paths. By using duplexers, antennas can be shared by both transmitters and receivers and thus the number of antennas can be reduced. The duplexer can be realized by different methods. One way is combining two bandpass filters with conventional matching network, usually T-junction or dual-mode resonator is used. However, because the size of matching network is closely related to the electrical length in the material, the capability of miniaturization is limited. Another way is using artificial transmission lines to generate different signal paths. Though the circuit size can be significantly reduced, the isolation level is usually a trade-off. Therefore, this thesis proposes a lumped element duplexer schematic which is the combination of cross-coupled bandpass filters and miniaturized matching network. Both high isolation level and small circuit size can be achieved.

After introducing the basic theory of the cross-coupled bandpass filter, a compensation method for non-ideal immittance inverter is proposed in this thesis. The mismatch in passband and frequency shifting can be compensated effectively by introducing more design degree of freedom, thus the lumped bandpass filter topology can be obtained. When two bandpass filters are finished, a lumped matching network can be applied to form a duplexer based on the theory in this thesis. The proposed duplexer achieves 50 dB isolation level with circuit size $0.072\lambda_g \times 0.038\lambda_g$. The proposed circuit has higher isolation level and can reach smaller size compared with several previous works.

Besides, a duplexer schematic for two close bands is also proposed. By introducing

both high-impedance path and low-impedance path, the isolation level can be improved. The proposed duplexer achieves 38 dB isolation level. Also, 30 dB suppression at GPS/Bluetooth bands is achieved by using the selective bandpass filter.
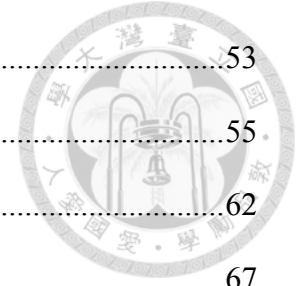
Index Terms — duplexer, matching network, isolation, lumped topology, miniaturization

CONTENTS

LIST OF FIGURES

LIST OF TABLES

Chapter 1   Introduction

1.1   Research Motivation

With the increasing demand for advanced communication technologies, much effort has been devoted to developing radio-frequency (RF) components with high performance, small footprints and low cost.

Duplexer is a three-port device and is one of the most basic components in frequency-division duplexing (FDD) system, in which channels are separated by different frequencies. Fig. 1.1 shows a simplified transceiver block diagram. By using duplexers, antennas can be shared by both transmitters (Tx) and receivers (Rx) and thus the number of antennas can be reduced. On the other hand, to ensure good transmission quality of both Tx and Rx, a well-designed duplexer shall achieve low insertion loss, sufficient isolation between Tx and Rx, and compact size.

In modern communication systems, Tx and Rx bands may be extremely closed to each other. For example, Tx and Rx bands of LTE band 1 are separated by only 10 % fractional bandwidth [1]. To keep good insertion loss and offer sufficient isolation, the selectivity of the duplexer is limited, or the order of the filters is pre-decided. However, when the losses of the structure are also considered, implementation of a high quality duplexer becomes a very challenging work.

Besides, one of the most important parts of a duplexer is the matching network. To ensure good isolation of two signal paths, the duplexer shall offer good in-band matching to each path in required bands and decouple the Tx and Rx path. Two most popular solutions for the matching designs are based on T-junction or common resonator topology. Nevertheless, both two structures are closely related to electrical length in the material, which makes miniaturization more difficult in the real design.

Compared to the transmission line based structure, lumped elements have the advantage of easier modeling and performance prediction in circuit level and much flexible size depending on the fitness of the process. Hence, this research aims to develop a full lumped-element duplexer with good isolation, good insertion loss and compact size.
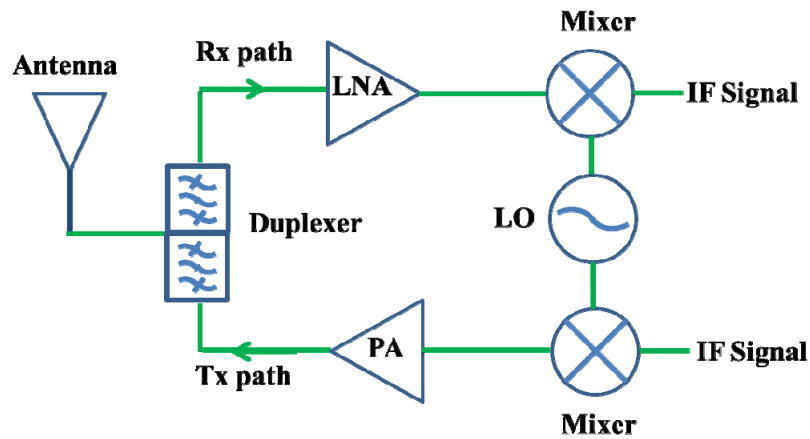
Fig. 1.1   Simplified transceiver block diagram

1.2   Literature Survey

A duplexer is capable of separating two signals of different frequency into different paths, thus can be considered as the combination of two bandpass filters with a matching network offering isolation between two paths. As mentioned before, the impedance matching at common port is critical for the circuit performance and there are two common solutions.

T-junction is one of the most popular matching networks in duplexer designs due to its simplicity [2]. T-junction schematic uses two 50 ohm transmission lines with certain electrical length to transform the finite input impedance of a bandpass filter into open circuit in order to achieve good matching to the other bandpass filter and offer good

isolation of Tx and Rx simultaneously, as demonstrated in Fig. 1.2, in which ω_1 and ω_2 are operation frequencies of filter 1 and filter 2, respectively. Based on T-junction schematic, plenty of structures are proposed to further enhance the performance of each band and reduce the total size [3]-[11]. In [3], half-wavelength and quarter-wavelength resonators are used simultaneously to introduce multiple transmission zeros (TZs), as shown in Fig. 1.3. Also, TZs can be generated due to cross-coupling between source and load [4]. In [5], dual-mode resonators are used for bandpass filter design, so the number of resonators can be reduced by half to reduce the total area. Duplexer based on slot resonators is proposed in [6]. The imperfect ground plane, however, may cause additional interference. The concept of signal-interference is applied in [7], in which good selectivity is achieved at the cost of circuit size. Other techniques for miniaturization of duplexer, such as high dielectric constant substrate [8], folded coupled-line structure [9] and multi-layer process [10], are also reported. Though many miniaturization techniques targeting on the bandpass filters have been proposed, the total size of the duplexer is still limited by the T-junction.
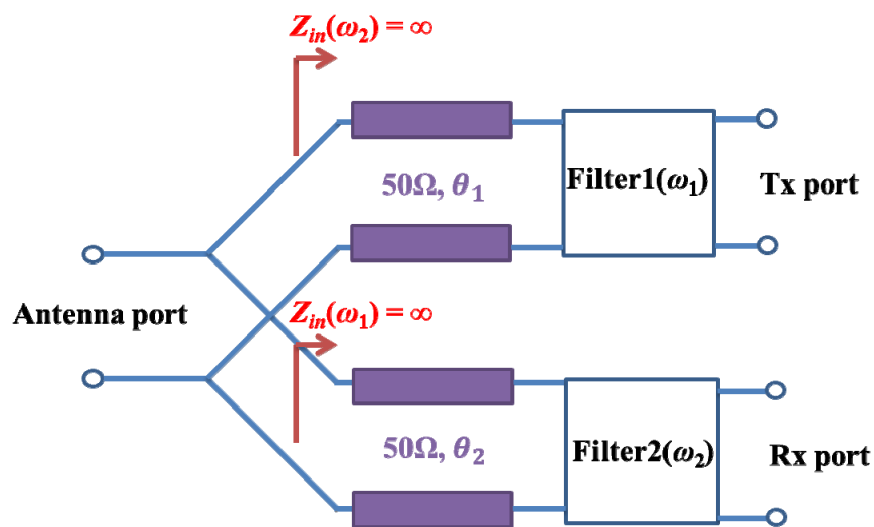
Fig. 1.2   Concept of T-junction topology
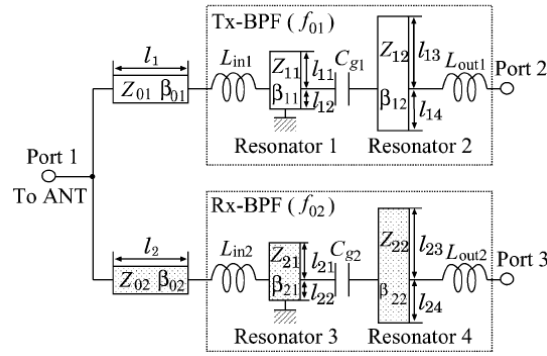
Fig. 1.3　The duplexer proposed in [3]

In addition to T-junction topology, common resonator tries to use parts of the filters to offer good isolation to avoid extra structure. The first common resonator topology is proposed in [11], which use a dual-mode resonator as the first stage of each bandpass filter to offer enough order of filter response in each path and achieve isolation at the same time, as demonstrated in Fig. 1.4. Since no extra structure exists and the number of resonator is reduced by one, the area of the duplexer can be reduced (Fig. 1.5). By applying this concept, [12] proposes a new composite right/left-handed transmission line resonator for further size reduction. Though miniaturization can be achieved in comparison with T-junction based topology, the bandwidth of two channels (Tx and Rx) cannot be controlled independently. In [13], a duplexer is implemented with tuning capabilities of center frequency and bandwidth of each band by using varactors.

Besides the conventional point of view, several very compact duplexers based on artificial transmission line can be found in [14]-[17]. Fig. 1.6 shows the structure in [14]. However, the isolation between two bands, is usually a trade-off. A compact LTCC duplexer for two close bands is proposed in [18], by using parallel LC tank to satisfy open circuit condition, the matching network can be eliminated.
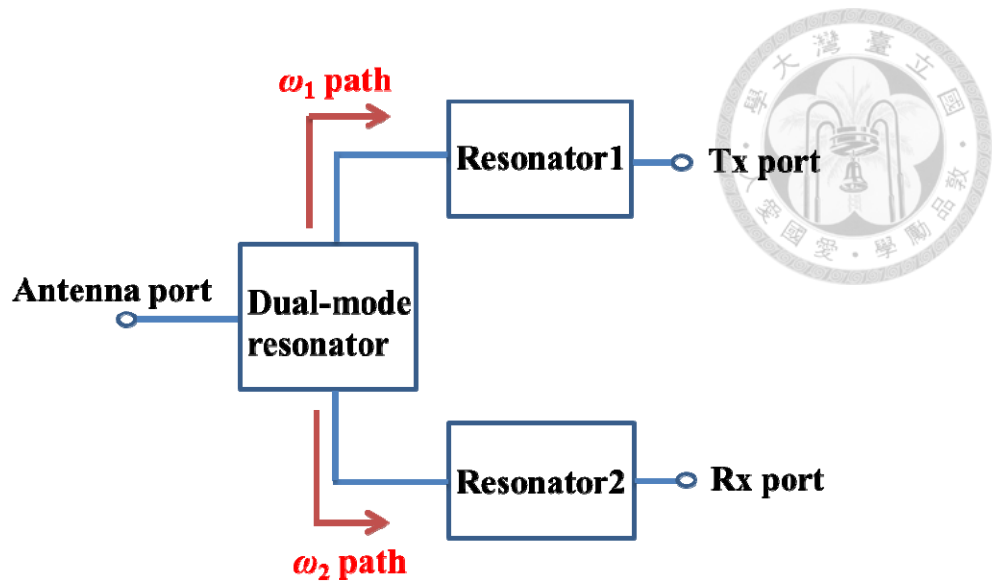
Fig. 1.4　Concept of common resonator topology
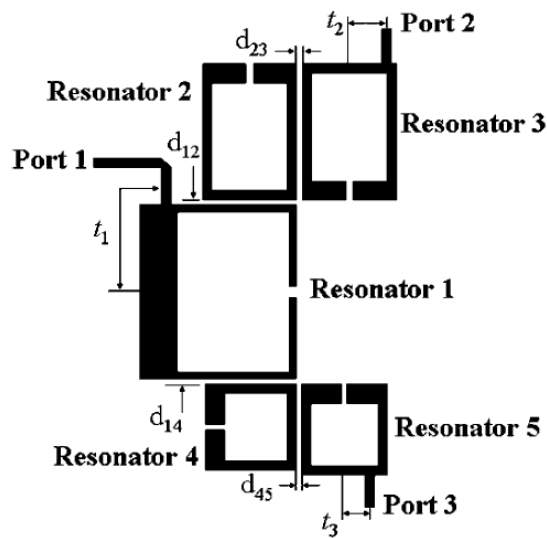
Fig. 1.5　The duplexer proposed in [11]
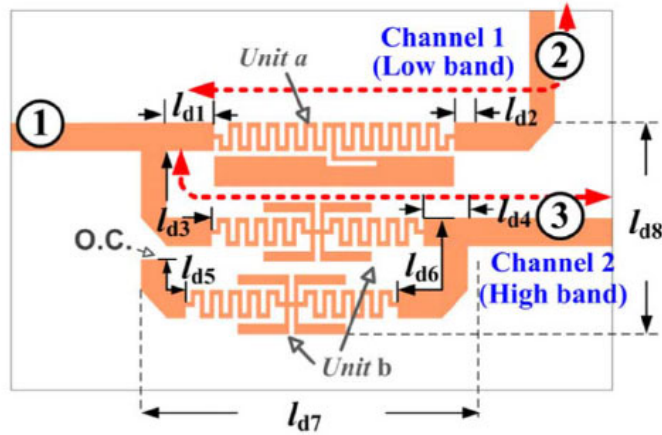
Fig. 1.6 The duplexer proposed in [14]

1.3 Contributions

A full lumped topology of a duplexer is proposed in this thesis, which contains a miniaturized matching network and two cross-coupled bandpass filters. The proposed matching network is suitable for combination of two bandpass filters. High isolation and compact size can be achieved simultaneously. Though the theory of cross-coupling has been well established [19], [20], it cannot be applied directly to lumped element design due to frequency dependency of immittance inverter. As a result, a method is proposed to compensate the effects of non-ideal immittance inverter.

Based on the structure in [18], a duplexer for two close bands is also proposed. TZs introduced by both high-impedance path and low-impedance path can offer higher isolation level than the previous work. Meanwhile, the bandpass filter in [18] is modified to provide isolation at GPS/Bluetooth bands.

1.4 Thesis Organization

The content of this thesis is organized as the follows. In Chapter 2, the basic theory of the third-order cross-coupled bandpass filter is introduced, and the compensation

method of non-ideal effects will be proposed.

Chapter 3 starts with general loading effects, and the corresponding matching networks will be investigated. Limitation of the proposed matching networks are also analyzed and improved by introducing higher-order circuits. Then, a duplexer is designed based on proposed matching network and bandpass filters in chapter 2. The circuit topology, simulated performance and the measured results will be given.

Chapter 4 starts with the basic theory and the design concept of the topology in [18]. The modified bandpass filter is then proposed for out-of-band rejection improvement. Also, the capability of isolation will be investigated and improved by the proposed bandstop structure. The circuit topology, simulated performance and the measured results will be shown. Finally, in chapter 5, conclusions of this thesis are given.

Chapter 2   Third-Order   Cross-Coupled   Bandpass

Filter

2.1   Basic Filter Theory

Filter is a frequency selective device and is the core parts in a duplexer. Fig. 2.1 shows four basic responses of filter, including low-pass, high-pass, band-pass and bandstop. Among those responses, bandpass response is the most common one since it can only let the desired frequency pass and get rid of other unwanted noise. According to the different requirement of the system, bandpass filter can be designed to meet many different functions, such as Butterworth, Chebyshev or elliptic response. In this chapter, we only focus on the synthesis flow of a bandpass filter with transmission zeros. Such flow can also base on different math functions depending on requirement.

Basically, a bandpass filter can be synthesized by the ladder topology [21], which is based on shunt and series resonators. However, sometimes such schematic is not practical in consideration of physical realization [22]. With the help of immittance inverter, only one kind of resonator is required to achieve the same response as the ladder circuit, as shown in Fig. 2.2.
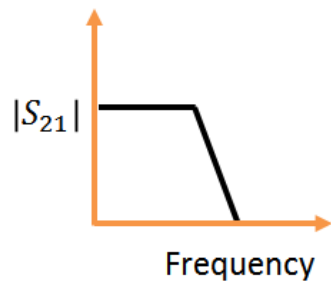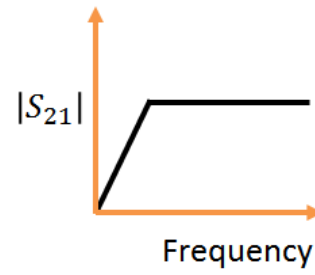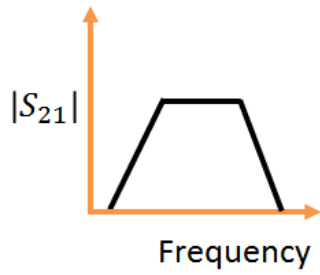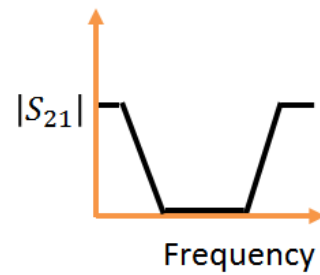
Fig. 2.1 Basic filter response (a) low-pass (b) high-pass (c) bandpass (d) bandstop
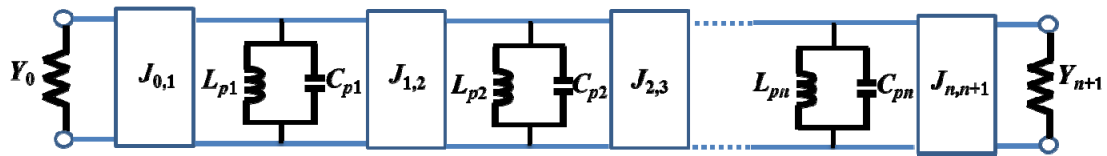
(a)
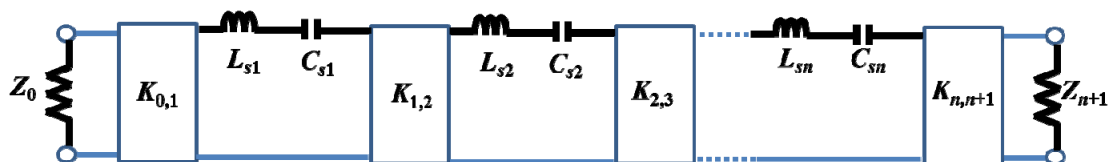
(b)

Fig. 2.2 Bandpass filter prototype based on (a) J-inverter (b) K-inverter

For prototype in Fig. 2.2(a), when the center frequency ω_0 and fractional bandwidth (*FBW*) are specified, the banspass filter with order of n can be constructed based on the following equations
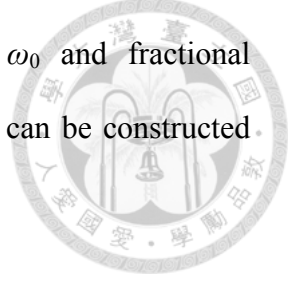
$$J_{0,1} = \sqrt{\frac{Y_0 FBW \omega_0 C_{p1}}{g_0 g_1}}, \tag{2.1}$$

$$J_{i,i+1} = FBW \omega_0 \sqrt{\frac{C_{pi} C_{p(i+1)}}{g_i g_{i+1}}}, \tag{2.2}$$

$$J_{n,n+1} = \sqrt{\frac{FBW \omega_0 C_{pn} Y_{n+1}}{g_n g_{n+1}}}, \tag{2.3}$$

$$L_{pi} = \frac{1}{\omega_0^2 C_{pi}}\bigg|_{i=1 \sim n}. \tag{2.4}$$

, where $g_{i,i=0 \sim n+1}$ are the element values of the specified response.

As for prototype in Fig. 2.2(b), when the center frequency ω_0 and fractional bandwidth (*FBW*) are specified, the banspass filter with order of n can be constructed based on the following equations

$$K_{0,1} = \sqrt{\frac{Z_0 FBW \omega_0 L_{s1}}{g_0 g_1}}, \tag{2.5}$$

$$K_{i,i+1} = FBW \omega_0 \sqrt{\frac{L_{si} L_{s(i+1)}}{g_i g_{i+1}}}, \tag{2.6}$$

$$K_{n,n+1} = \sqrt{\frac{FBW \omega_0 L_{sn} Z_{n+1}}{g_n g_{n+1}}}, \tag{2.7}$$

$$C_{pi} = \frac{1}{\omega_0^2 L_{pi}}\bigg|_{i=1 \sim n}. \tag{2.8}$$

, where $g_{i,i=0\sim n+1}$ are the element values of the specified response.

Duality can be observed between two prototypes. The inverter-based prototypes mentioned above are more flexible than conventional ladder topology. For example, the even-order Chebyshev response is not practical for ladder topology due to unsymmetrical impedance condition, inverter-based prototypes, on the contrary, can be easily designed in symmetric schematic with both ports impedance being the same.

In Fig. 2.2, every interaction between resonators and source/load is modeled as *J* or *K* inverter. Notice that this topology is only valid for narrow-band application since ideal immittance inverter is not practical. There are numerous circuits that can realize immittance inverter [22]. Some common choices are listed in Fig. 2.3.

$$K = \omega L$$

(a)

$$K = \frac{1}{\omega C}$$

(b)

$$J = \frac{1}{\omega L}$$

(c)

$$J = \omega C$$

(d)

$$K = Z_o \tan\left|\frac{\theta}{2}\right|$$

$$\theta = -\tan^{-1}\left|\frac{2X}{Z_o}\right|$$

$$X = \omega L$$

$$X = -\frac{1}{\omega C}$$

$$\left|\frac{X}{Z_o}\right| = \frac{K/Z_o}{1-(K/Z_o)^2}$$

(e)

(f)

$$J = Y_o \tan\left|\frac{\theta}{2}\right|$$

$$\theta = -\tan^{-1}\left|\frac{2B}{Y_o}\right|$$

$$B = -\frac{1}{\omega L}$$

$$B = \omega C$$
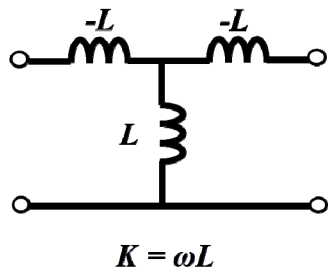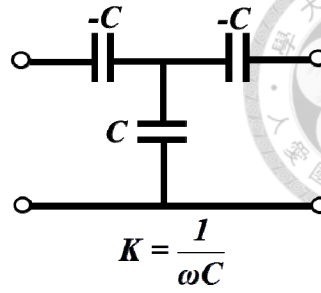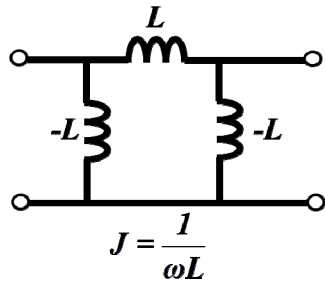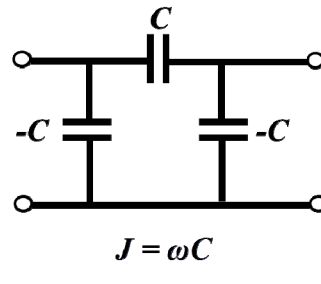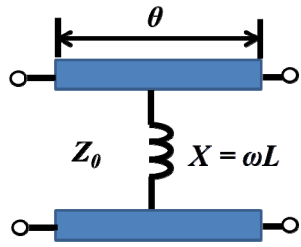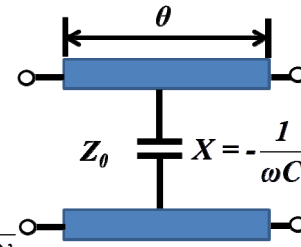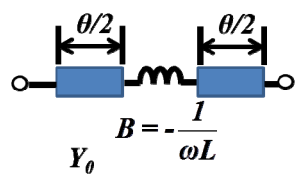
$$\left|\frac{B}{Y_o}\right| = \frac{J/Y_o}{1-(J/Y_o)^2}$$

(g)
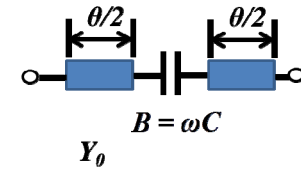
(h)

Fig. 2.3　Various circuits for implementation of immittance inverter (a)-(h)

In consideration of circuit compactness, immittance inverters based on full lumped elements are usually preferred. Due to duality of *J/K*-inverter, only *J*-inverter is analyzed below for further discussion. To realize a *J*-inverter by using lumped elements, the π-model can be adopted, as shown in Fig. 2.3(c)-(d). For ideal *J*-inverter, its *ABCD* matrix can be written as

$$\begin{bmatrix} A & B \\ C & D \end{bmatrix} = \begin{bmatrix} 0 & \pm\dfrac{1}{\mathrm{j}J} \\ \mp\mathrm{j}J & 0 \end{bmatrix}. \tag{2.9}$$

Where the $\pm$ sign represents $\pm 90°$ phase shifting. For circuit shown in Fig. 2.3(d), the *ABCD* matrix is

$$\begin{bmatrix} A & B \\ C & D \end{bmatrix} = \begin{bmatrix} 1 & 0 \\ -\mathrm{j}\omega C & 1 \end{bmatrix}\begin{bmatrix} 1 & \dfrac{1}{\mathrm{j}\omega C} \\ 0 & 1 \end{bmatrix}\begin{bmatrix} 1 & 0 \\ -\mathrm{j}\omega C & 1 \end{bmatrix} = \begin{bmatrix} 0 & \dfrac{1}{\mathrm{j}\omega C} \\ -\mathrm{j}\omega C & 0 \end{bmatrix} = \begin{bmatrix} 0 & \dfrac{1}{\mathrm{j}J} \\ -\mathrm{j}J & 0 \end{bmatrix}, \tag{2.10}$$

Thus we get the value of *J*-inverter as

$$J = \omega C. \tag{2.11}$$

As for circuit shown in Fig. 2.3(c), the *ABCD* matrix can be given as

$$\begin{bmatrix} A & B \\ C & D \end{bmatrix} = \begin{bmatrix} 1 & 0 \\ \dfrac{-1}{\mathrm{j}\omega L} & 1 \end{bmatrix}\begin{bmatrix} 1 & \mathrm{j}\omega L \\ 0 & 1 \end{bmatrix}\begin{bmatrix} 1 & 0 \\ \dfrac{-1}{\mathrm{j}\omega L} & 1 \end{bmatrix} = \begin{bmatrix} 0 & \mathrm{j}\omega L \\ \dfrac{-1}{\mathrm{j}\omega L} & 0 \end{bmatrix} = \begin{bmatrix} 0 & -\dfrac{1}{\mathrm{j}J} \\ \mathrm{j}J & 0 \end{bmatrix}, \tag{2.12}$$

13

The value of *J*-inverter can then be obtained as

$$J = \frac{1}{\omega L}.$$

Obviously, two inverters based on capacitors and inductors are out of phase, and they are conventionally referred to as electric coupling and magnetic coupling, respectively.

It is interesting to note that *C* and *L* here are positive values in practice since only shunt elements can be absorbed into adjacent resonators. In fact, *L* can be implemented physically for both positive and negative values by using the equivalent circuit shown in Fig. 2.4, which can be proved by equating their *Y* parameter.

$$L_A = \frac{L_1 L_2 - M^2}{L_2 - M}, \qquad L_B = \frac{L_1 L_2 - M^2}{L_1 - M}$$
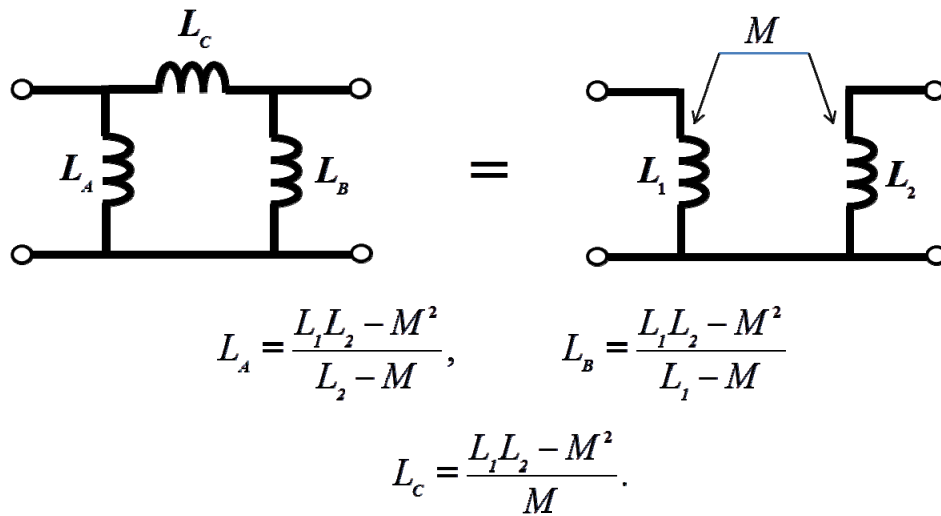
$$L_C = \frac{L_1 L_2 - M^2}{M}.$$

Fig. 2.4   Equivalent circuit for coupled inductors

By controlling the sign of mutual inductance *M*, both positive and negative values of *L* are realizable. However, since no such equivalent circuit exists for electric coupling, negative *C* is not practical.

2.2   Modeling of Third-Order Bandpass Filter with Cross-Coupling

Based on conventional filter topology, more advanced response can be obtained by introducing cross-coupling. General filter structure with cross-coupling can be completely described by the coupling matrix [19]. Nevertheless, to ensure transmission zeros at desired frequencies, sometimes complicated mathematical techniques are required for solving iteration equations.

In addition, cross-coupling may also disturb the response in the desired band. To more specific, for a Chebyshev bandpass filter with the existence of cross-coupling, the equal-ripple response in the passband will be disturbed, and therefore the insertion loss cannot be ensured anymore. To compensate such effect, [23] proposes a modified fourth-order cross-coupled bandpass filter as an example. Two inverters at source and load are modified to recover impedance matching at center frequency. This method, however, is suitable only for filter of even order due to the simplification method of cascaded J inverters used in the research.

As far as we know, selectivity of the filter can be improved by increasing its order at the cost of total loss because of the increasing elements. In some cases, even-order filter design is not sufficient considering the selectivity and loss together. Therefore, to construct a possible compensation method for odd-order bandpass filter with cross-coupling is important. In consideration of the simplicity and the real application, in this chapter we only focus on third-order designs.

2.2.1   Ideal Circuit Model

Fig. 2.5(a) shows the third-order bandpass filter prototype, a filter of Chebyshev

response is designed for demonstration and shown in Fig. 2.5(b) with the specification

listed in Table 2.1.

Table 2.1 Specification of the filter

Ripple	ω_0	FBW
0.1 dB	1.733 GHz	6 %
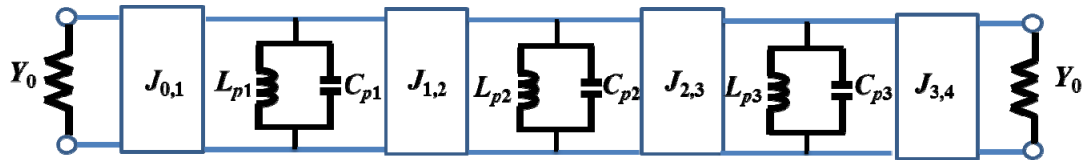
(a)
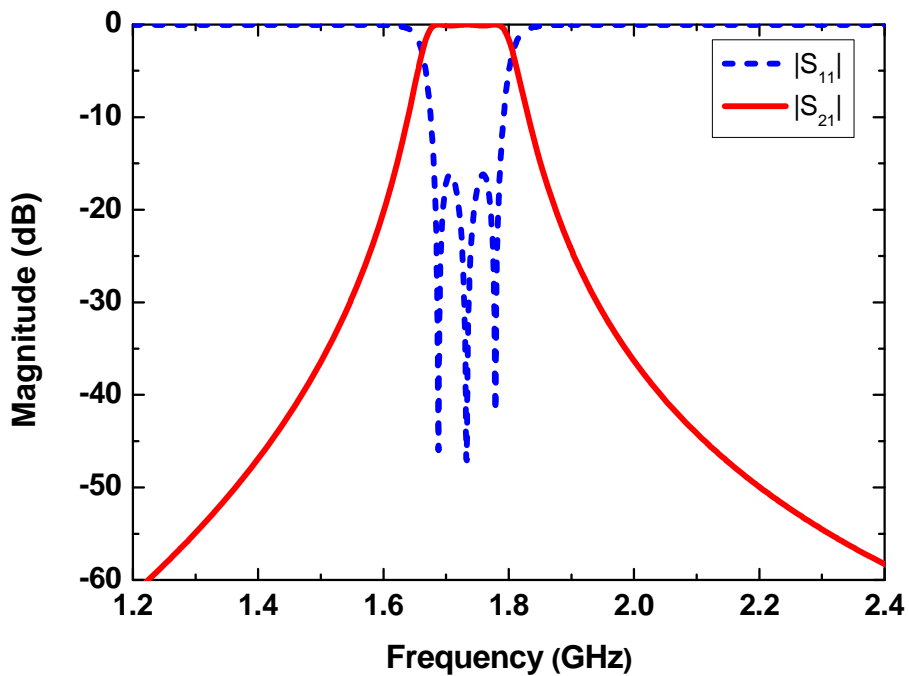
(b)

Fig. 2.5   Third-order bandpass filter (a) circuit topology (b) response
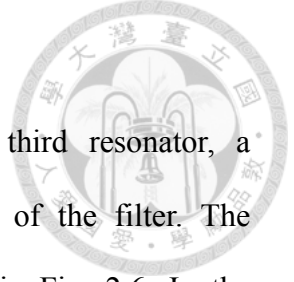
Transmission Zeros and Cross-coupling

By introducing cross-coupling between the first and the third resonator, a transmission zero (TZ) can be generated to improve selectivity of the filter. The cross-coupling effect can be modeled as a *J*-inverter, as shown in Fig. 2.6. In the following discussion, we denote the signs of electric coupling and magnetic coupling are positive and negative, respectively.
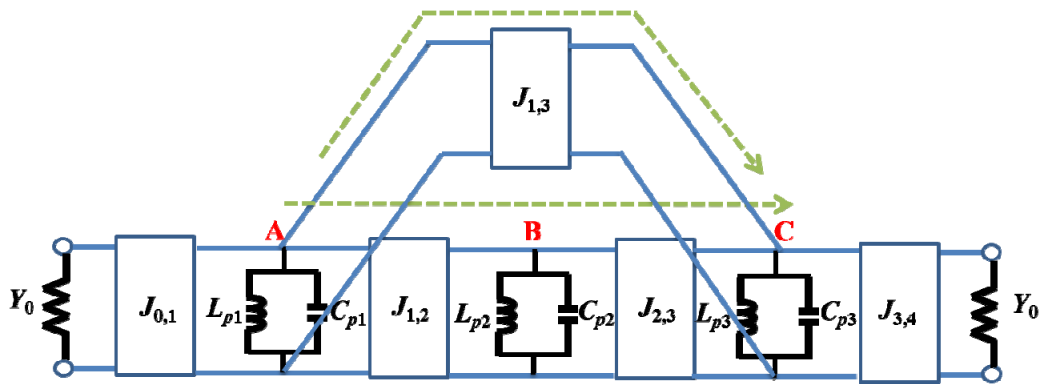
Fig. 2.6　Third-order bandpass filter with cross-coupling between node A and C

The TZ condition can be analyzed by *Y*-parameter of two signal paths. For ideal *J*-inverter, its *ABCD* matrix can be written as

$$\begin{bmatrix} A & B \\ C & D \end{bmatrix} = \begin{bmatrix} 0 & \dfrac{1}{\mathrm{j}J} \\ -\mathrm{j}J & 0 \end{bmatrix}, \tag{2.14}$$

For a shunt susceptance $B(\omega)$, its *ABCD* matrix is

$$\begin{bmatrix} A & B \\ C & D \end{bmatrix} = \begin{bmatrix} 1 & 0 \\ \mathrm{j}B(\omega) & 1 \end{bmatrix}, \tag{2.15}$$

17

Therefore, the *ABCD* matrix of path ABC can be represented as

$$\begin{bmatrix} A & B \\ C & D \end{bmatrix} = \begin{bmatrix} 0 & \dfrac{1}{\mathrm{j}J_{12}} \\ -\mathrm{j}J_{12} & 0 \end{bmatrix} \begin{bmatrix} 1 & 0 \\ \mathrm{j}B_2(\omega) & 1 \end{bmatrix} \begin{bmatrix} 0 & \dfrac{1}{\mathrm{j}J_{23}} \\ -\mathrm{j}J_{23} & 0 \end{bmatrix} = \begin{bmatrix} -\dfrac{J_{23}}{J_{12}} & \dfrac{B_2(\omega)}{\mathrm{j}J_{12}J_{23}} \\ 0 & -\dfrac{J_{12}}{J_{23}} \end{bmatrix}. \quad (2.16)$$

Where $B_2(\omega)$ is the susceptance of the second resonator. As for path AC, its *ABCD* matrix can be written as

$$\begin{bmatrix} A & B \\ C & D \end{bmatrix} = \begin{bmatrix} 0 & \dfrac{1}{\mathrm{j}J_{13}} \\ -\mathrm{j}J_{13} & 0 \end{bmatrix}. \quad (2.17)$$

The Y_{12} parameter of two signal paths can then be obtained as

$$Y_{21\_\mathrm{ABC}} = \frac{-\mathrm{j}J_{12}J_{23}}{B_2(\omega)}, \quad (2.18)$$

$$Y_{21\_\mathrm{AC}} = -\mathrm{j}J_{13}. \quad (2.19)$$

TZ will be generated when

$$Y_{21\_\mathrm{ABC}} + Y_{21\_\mathrm{AC}} = 0. \quad (2.20)$$

Finally the cross-coupling element is

$$J_{13} = \frac{-J_{12}J_{23}}{B_2(\omega)}.$$

(2.21)

Equation (2.21) states that the frequency of TZ depends on not only the coupling strength of each resonator but also the sign of coupling. Two filters are designed for demonstration with the specification listed in Table 2.2, and the related circuit parameters are listed in Table 2.3, which are calculated based on synthesis procedure discussed above. Fig. 2.7 shows TZ can be generated at either lower or higher frequency according to the design of the cross-coupling.

Table 2.2 Specification of the cross-coupled filters

	Ripple	ω_0	*FBW*	TZ
Filter 1	0.1 dB	1.733 GHz	6 %	1.924 GHz
Filter 2	0.1 dB	2.133 GHz	6 %	1.975 GHz

Table 2.3 Related circuit parameters

Filter 1			Filter 2		
C_{p1} (pF)	C_{p2} (pF)	C_{p3} (pF)	C_{p1} (pF)	C_{p2} (pF)	C_{p3} (pF)
12	6	12	8	6	8
L_{p1} (nH)	L_{p2} (nH)	L_{p3} (nH)	L_{p1} (nH)	L_{p2} (nH)	L_{p3} (nH)
0.70325	1.40650	0.70325	0.69626	0.92835	0.69626
J_{01}	J_{12}	J_{23}	J_{01}	J_{12}	J_{23}
0.0123	-0.0051	-0.0051	0.0112	-0.0051	0.0051
J_{34}	J_{13}		J_{34}	J_{13}	
0.0123	-0.0019		0.0112	-0.0021	
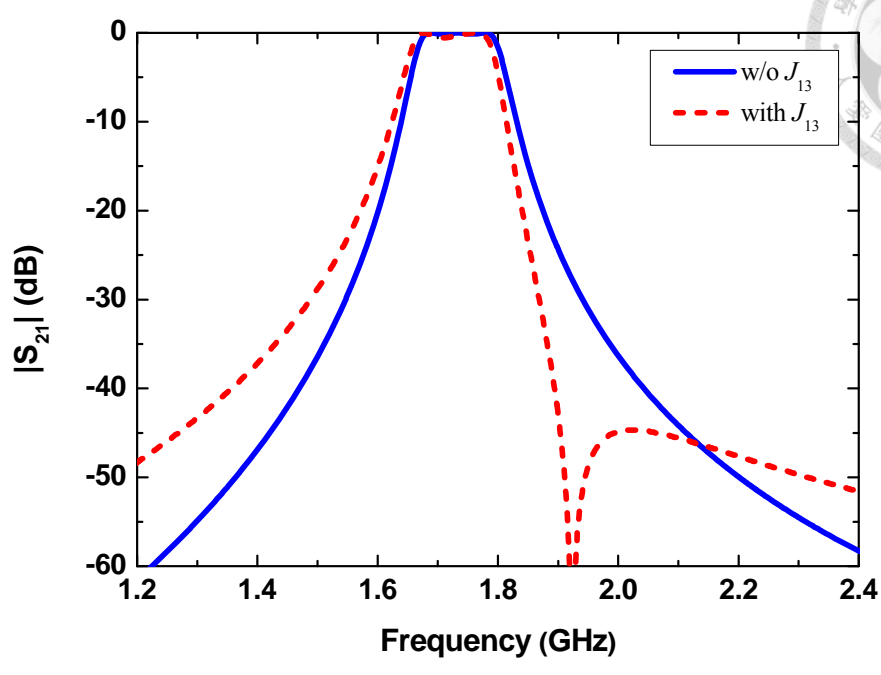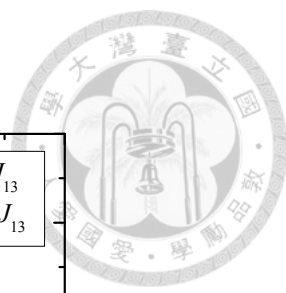
(a)
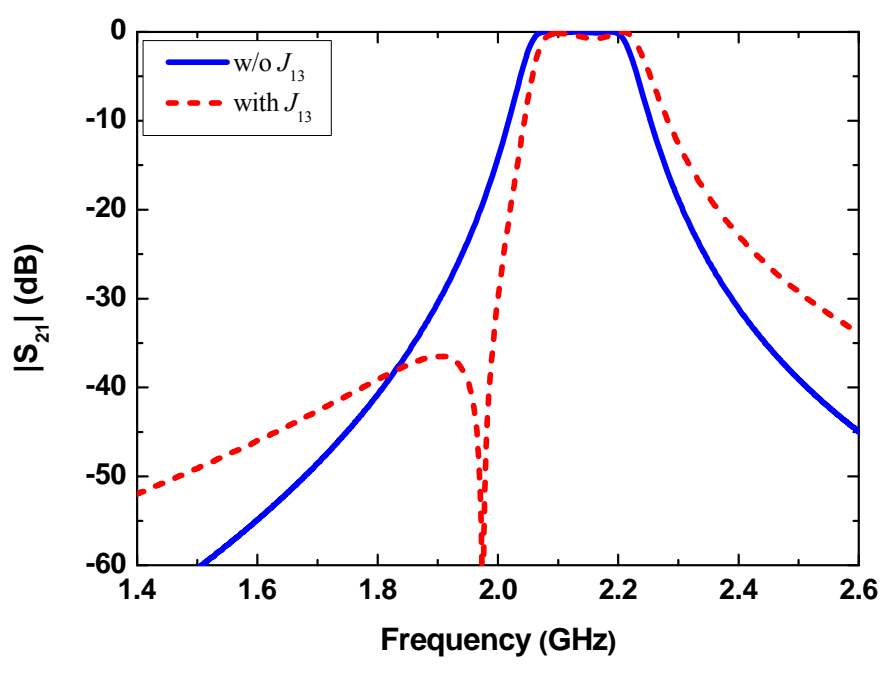
(b)

Fig. 2.7 Filter responses with cross-coupling (a) Filter 1 (b) Filter 2
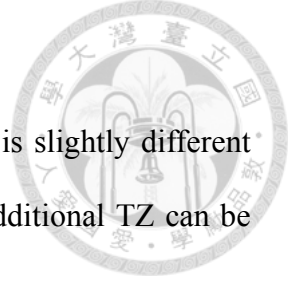
Source-load coupling

If a coupling between source and load is introduced, the case is slightly different from other cross-couplings. For a source-load coupling, a pair of additional TZ can be generated [20], as shown in Fig. 2.8.
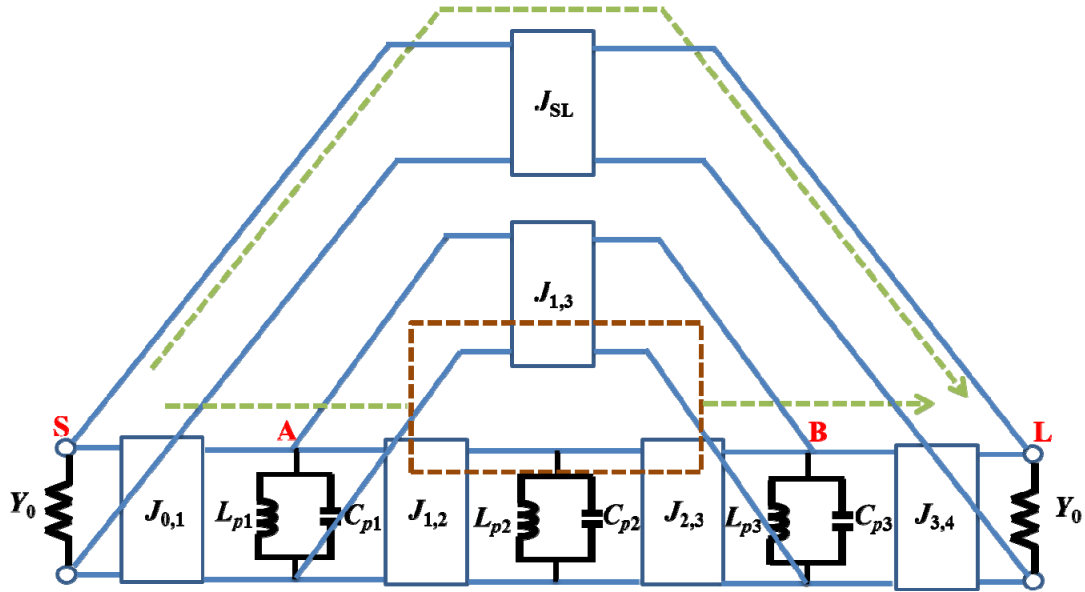
Fig. 2.8   Filter topology with cross-coupling and source-load coupling

TZ will be generated if

$$Y_{21\_SABL} + Y_{21\_SL} = 0. \tag{2.22}$$

Thus the source-load coupling can be derived as

$$J_{SL} = \frac{-(J_{01}J_{12}J_{23}J_{34} + J_{01}J_{34}J_{13}B_2(\omega))}{B_1(\omega)B_2(\omega)B_3(\omega) - J_{13}^2(B_1(\omega) + B_2(\omega)) - J_{12}^2 B_3(\omega) - 2J_{12}J_{23}J_{13}}. \tag{2.23}$$
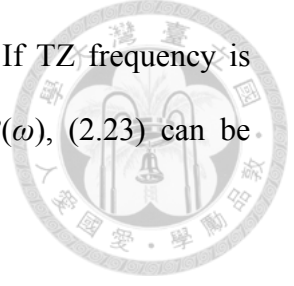
Where $B_1(\omega)$, $B_2(\omega)$ and $B_3(\omega)$ are susceptances of the resonator. If TZ frequency is away from the center frequency and assume $B_1(\omega) = B_3(\omega) = B(\omega)$, (2.23) can be simplified as

$$J_{SL} = \frac{-J_{01}J_{34}J_{13}}{B^2(\omega)}. \qquad (2.24)$$

For demonstration purpose, source-load coupling is introduced based on the circuit parameters listed in Table 2.3, and the responses are shown in Fig. 2.9 and Fig. 2.10. As can be seen, two additional TZs are generated which significantly enhance the out-band rejection.
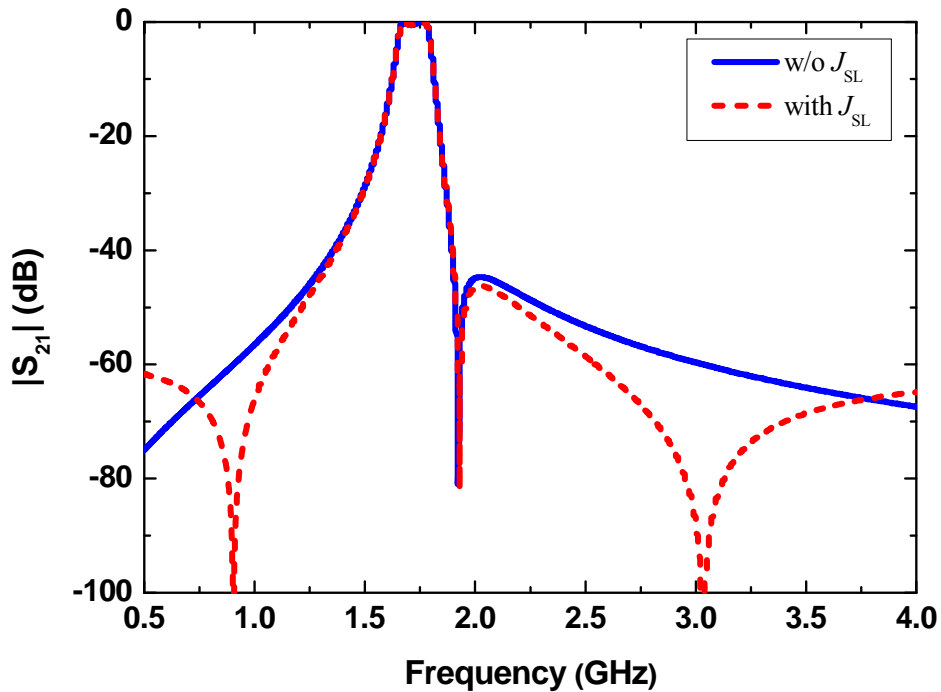
Fig. 2.9　Filter response with cross-coupling and source-load coupling--Filter 1
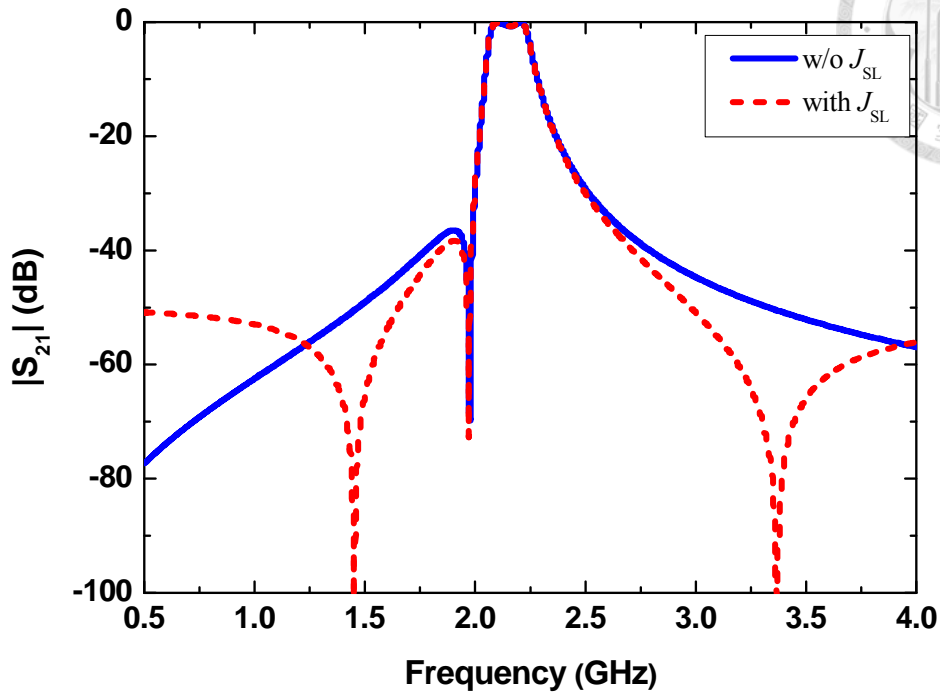
Fig. 2.10 Filter response with cross-coupling and source-load coupling--Filter 2

2.2.2 Compensation Method for Non-ideal *J*-inverter

Though the circuit model shown in Fig. 2.8 is mathematically correct, ideal *J*-inverter is not practical in real world. To convert the ideal model into realistic lumped circuit, *J*-inverters in Fig. 2.3 will be adopted as an example, and only a series inductor or a series capacitor is used for modeling the cross-coupling effect without affecting the TZ frequency.

Fig. 2.11 shows the lumped circuit of third-order bandpass filter with cross-coupling and source-load coupling. Notice that *J*-inverters at the source and load are modified since circuit elements of negative value cannot be absorbed here [24]. The modified equations are given as

23

$$C_{1m} = \frac{J_{01}}{\omega_0 \sqrt{1-(\frac{J_{01}}{Y_0})^2}}, \qquad (2.25)$$

$$C_{2m} = \frac{-C_{1m}Y_0}{Y_0^2 + \omega_0^2 C_{1m}^2}, \qquad (2.26)$$

$$C_{3m} = \frac{J_{34}}{\omega_0 \sqrt{1-(\frac{J_{34}}{Y_0})^2}}, \qquad (2.27)$$

$$C_{4m} = \frac{-C_{3m}Y_0}{Y_0^2 + \omega_0^2 C_{3m}^2}. \qquad (2.28)$$
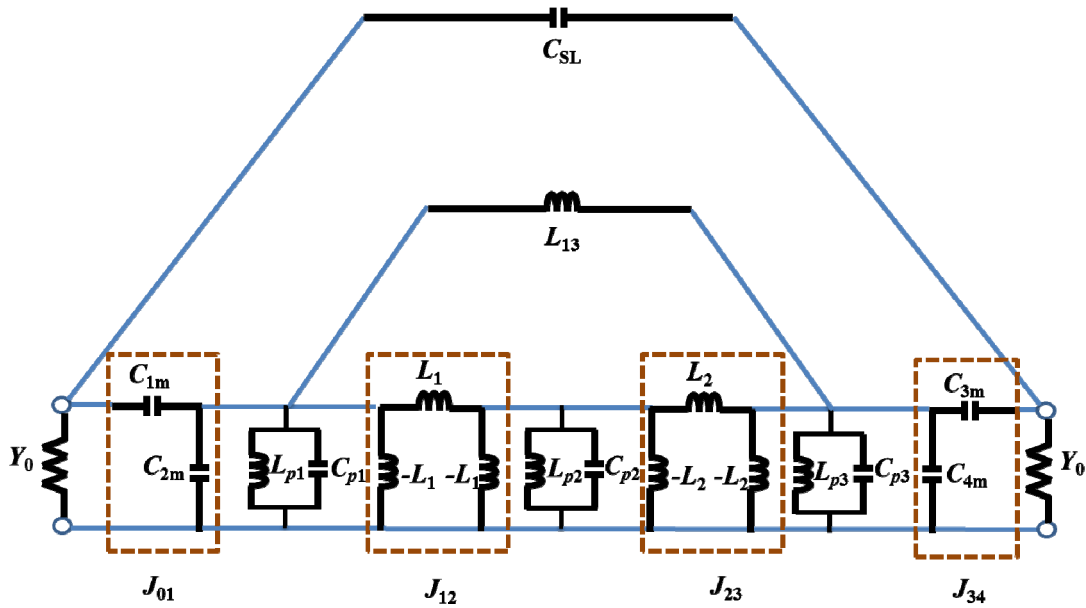
Fig. 2.11 A lumped model of third-order cross-coupled bandpass filter

Frequency shift and impedance mismatch in passband may be caused due to the frequency-dependency of J-inverters and the cross-coupling, which are usually undesired. The theory of coupling matrix can be only applied on frequency-invariant J-inverters [19], therefore, a method is proposed to compensate this effect. Since the Chebyshev filter can be constructed by symmetrical circuit topology, we let

$$J_{01} = J_{34}, \tag{2.29}$$

$$J_{12} = \pm J_{23}, \tag{2.30}$$

$$C_{p1} = C_{p3}, \tag{2.31}$$

$$L_{p1} = L_{p3}, \tag{2.32}$$

Notice that the minus sign in (2.30) will not affect the symmetry of the topology if we convert the second resonator from shunt LC tank into series LC tank.

As shown in Fig. 2.12, by introducing more design degree of freedom, which are C_{p1m}, C_1 and C_2, along with two cross-coupling elements C_{SL} and L_{13}, the following equations can be solved simultaneously based on even and odd mode analysis

$$Y_{even}(\omega_{p1}) * Y_{odd}(\omega_{p1}) = Y_0^2, \tag{2.33}$$

$$Y_{even}(\omega_{p2}) * Y_{odd}(\omega_{p2}) = Y_0^2, \tag{2.34}$$

$$Y_{even}(\omega_{p3}) * Y_{odd}(\omega_{p3}) = Y_0^2, \tag{2.35}$$

$$Y_{even}(\omega_{z1}) = Y_{odd}(\omega_{z1}), \tag{2.36}$$

$$Y_{even}(\omega_{z2}) = Y_{odd}(\omega_{z2}). \tag{2.37}$$

Where ω_{p1}, ω_{p2}, and ω_{p3} are reflection zeros and ω_{z1} and ω_{z2} are specified TZs. Y_{even} and Y_{odd} are the input admittance of even mode and odd mode of filter circuit, respectively. The design flow of the compensation to third-order cross-coupled bandpass filter is shown in Fig. 2.13.

$$L_{p1m} = \frac{1}{\omega_0^2 C_{p1m}}$$
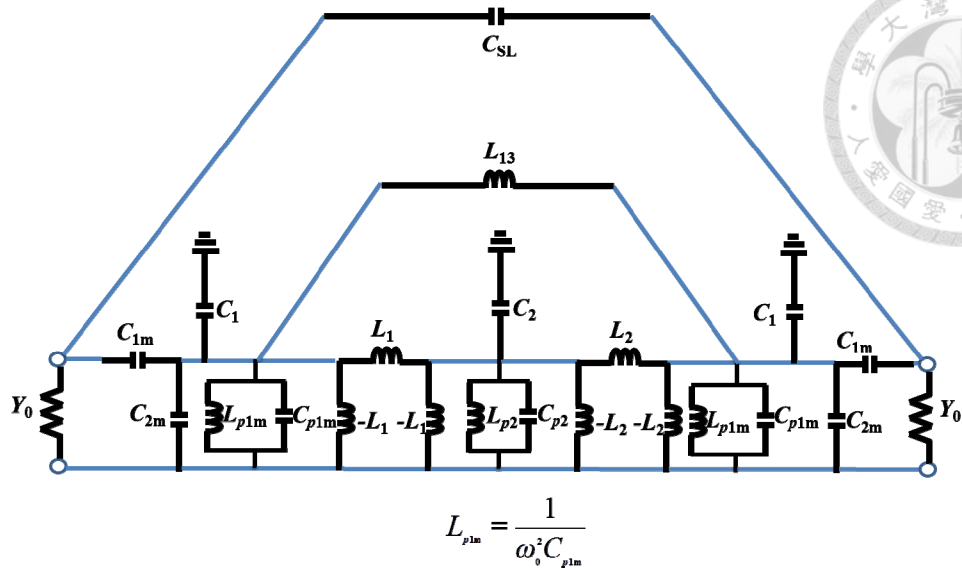
Fig. 2.12 A lumped model with compensation of frequency-dependency

Give ω_0 and *FBW* of the filter.

Design a traditional third-order bandpass filter with Chebyshev response.

Convert the ideal bandpass filter into full lumped circuit.

Solve equation(2.33)-(2.37) by using three reflection zeros and two specified TZs.

Modify the circuit topology with new circuit elements.

Done.

Fig. 2.13 Design flow of the compensated bandpass filter

Based on the design flow described in Fig. 2.13, two filters are designed for demonstration with the specification listed in Table 2.4, and Table 2.5 lists the compensated circuit parameters. Impedance matching in passband can be effectively recovered, as shown in Fig. 2.14 and F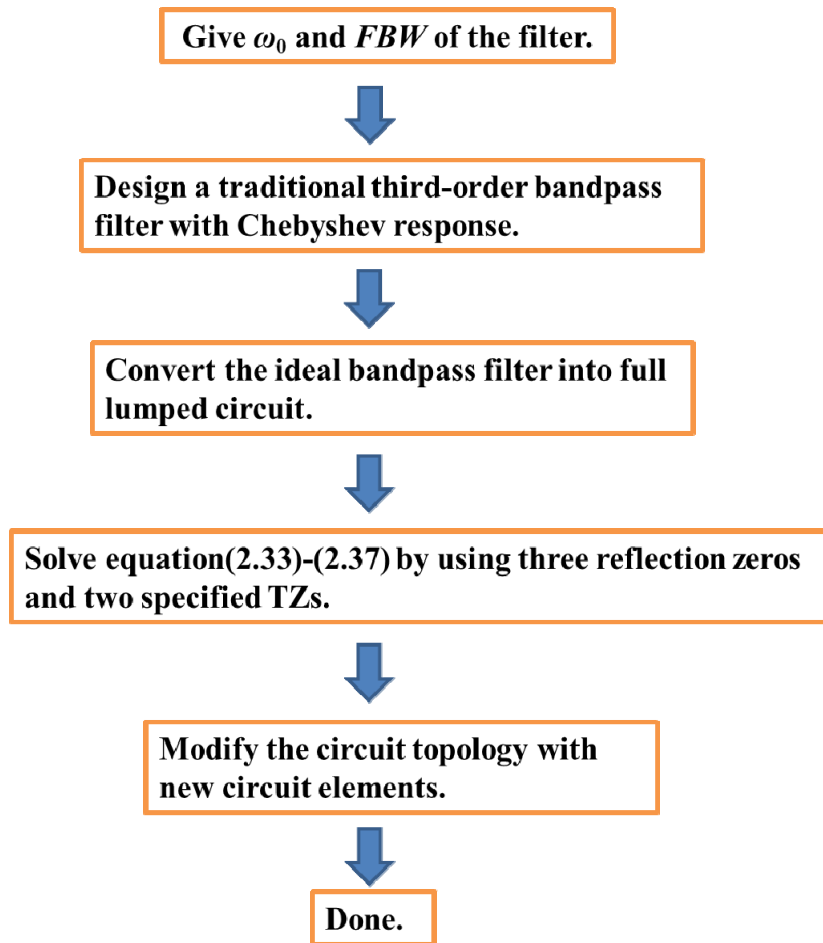ig. 2.15. In Fig. 2.14 and Fig. 2.15, the ideal Chebyshev filter without cross-coupling and the cross-coupled bandpass filter with and without compensation are compared. Both good insertion loss and selectivity are achieved in compensated case.

Table 2.4 Specification of the filters with source-load coupling and cross-coupling

	Ripple	ω_0	*FBW*	TZ_1	TZ_2
Filter 1	0.1 dB	1.733 GHz	6 %	1.94 GHz	2.133 GHz
Filter 2	0.1 dB	2.133 GHz	6 %	1.94 GHz	1.733 GHz

Table 2.5 Compensated circuit parameters

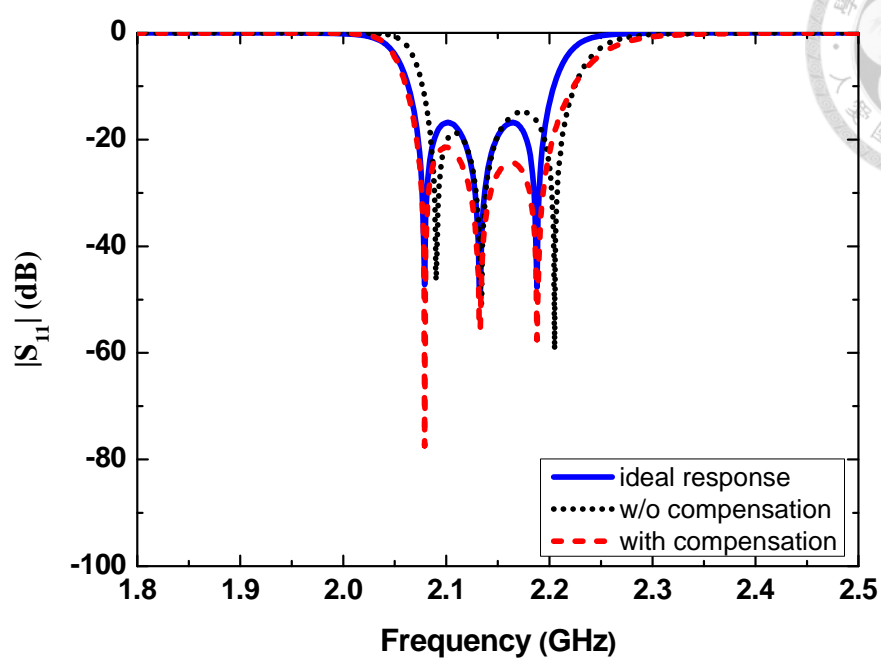| Filter 1			Filter 2		
C_{p1m} (pF)	C_{p2} (pF)	C_1 (pF)	C_{p1m} (pF)	C_{p2} (pF)	C_1 (pF)
7	6	0.24	5.9	6	0.0675
C_2 (pF)	C_{1m} (pF)	C_{2m} (pF)	C_2 (pF)	C_{1m} (pF)	C_{2m} (pF)
-0.18432	1.438	-0.89174	0.0892	1.0045	-0.6914
C_{SL} (pF)	L_{p1m} (nH)	L_{p2} (nH)	C_{SL} (pF)	L_{p1m} (nH)	L_{p2} (nH)
0.021	1.20558	1.4065	0.0175	0.94408	0.92835
L_1 (nH)	L_2 (nH)	L_{13} (nH)	L_1 (nH)	L_2 (nH)	L_{13} (nH)
18.034	18.034	39.36	-14.578	14.578	34.39
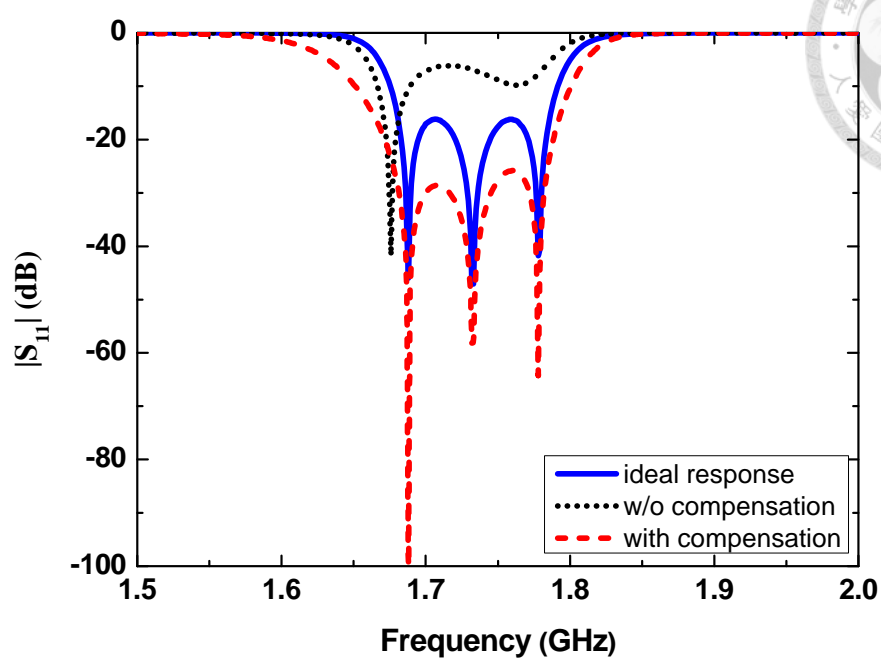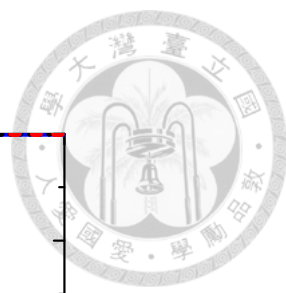
(a)
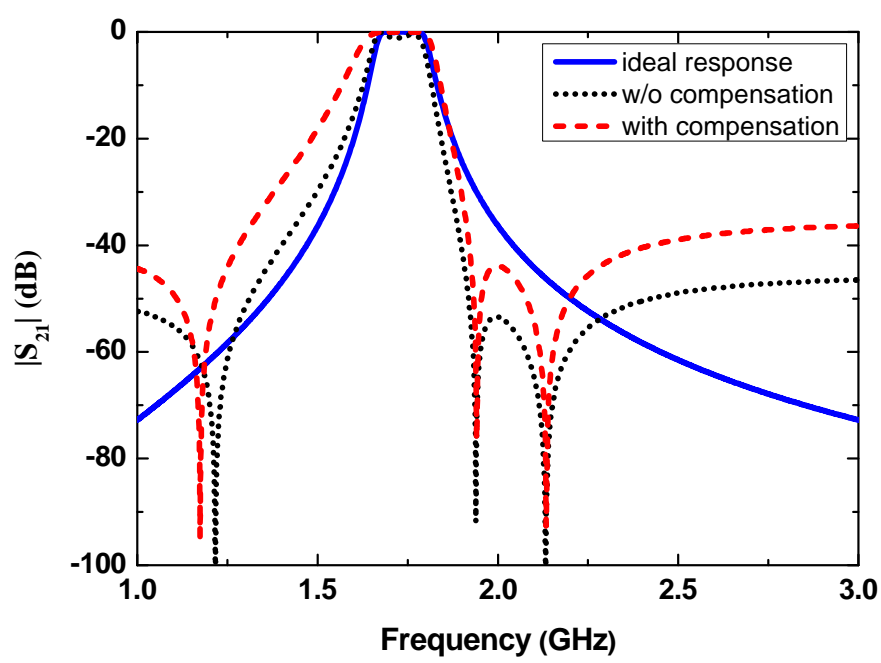
(b)

Fig. 2.14 Compensated responses of filter 1 (a) $|S_{11}|$ (b) $|S_{21}|$
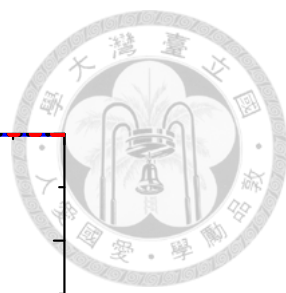
(c)
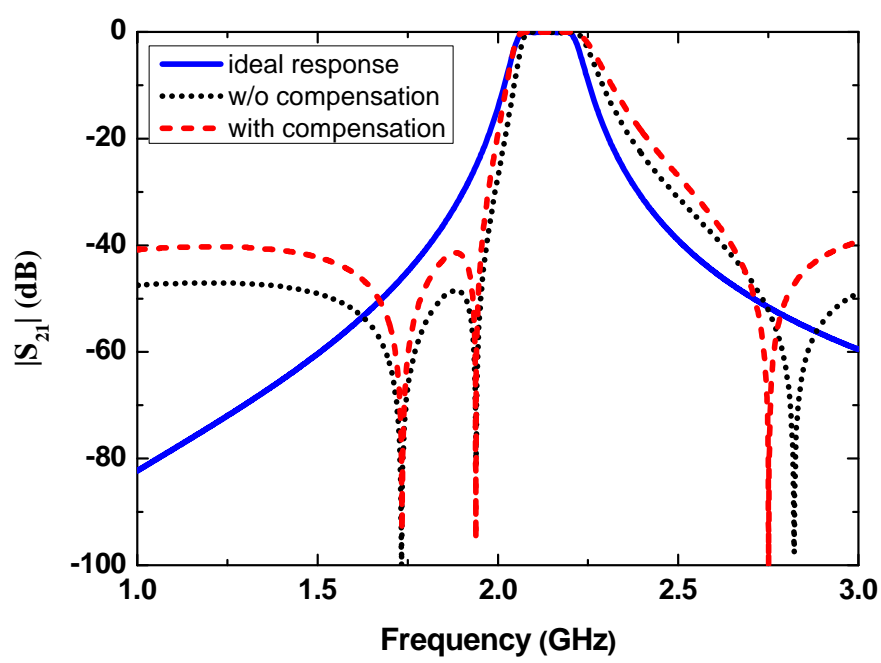
(d)

Fig. 2.15 Compensated responses of filter 2 (a) $|S_{11}|$ (b) $|S_{21}|$

2.3　Summary

In this chapter, basic filter theory has been introduced, including conventional topology and concept of cross-coupling. By allowing more design degree of freedom, mismatch in passband and frequency shifting can be recovered effectively based on the proposed design flow.

Chapter 3   Miniaturized Duplexer Design

3.1   Miniaturized Matching Network

Generally, a TZ is usually generated by open or short circuit, which means that the input admittance of the filter is zero or infinity. However, for a cross-coupled bandpass filter, its input admittance is pure imaginary at the TZ frequency. Fig. 3.1 and Fig. 3.2 show the input admittance of filters designed in chapter 2. As can be seen, the real part is zero while the imaginary part is a finite value at the TZ frequency.
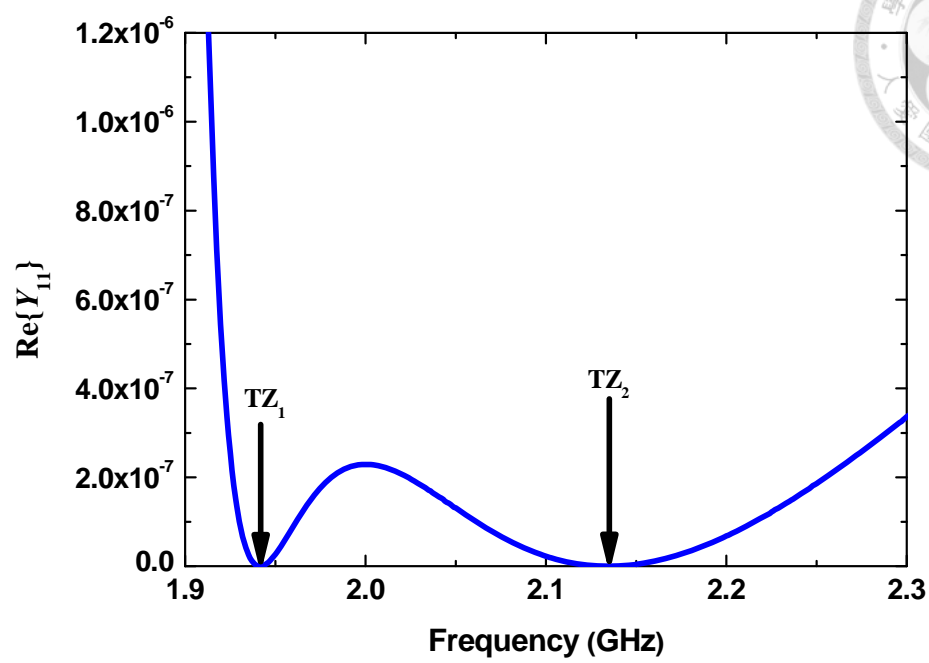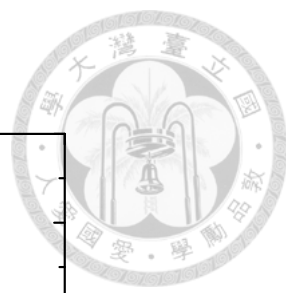
(a)
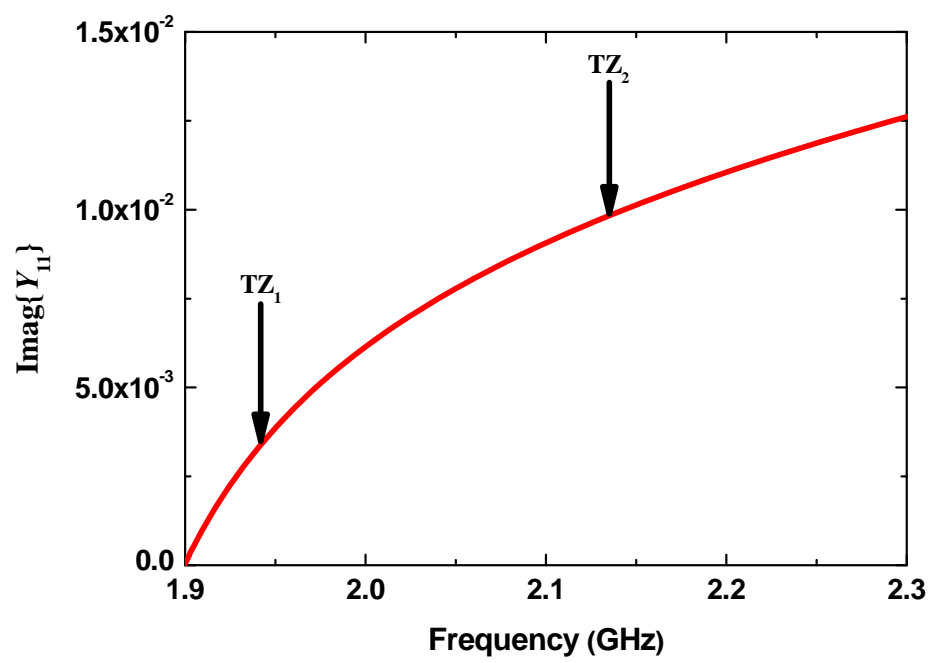
(b)

Fig. 3.1   Input admittance of filter 1 (a) real part (b) imaginary part

(a)

(b)

Fig. 3.2   Input admittance of filter 2 (a) real part (b) imaginary part

If both filters are designed to have a TZ at each other's bands, the finite imaginary input admittance of filter can be considered as a loading element at TZ frequency. Since the loading element may be capacitive or inductive, there are four possible combinations for loading element, as shown in Table 3.1.

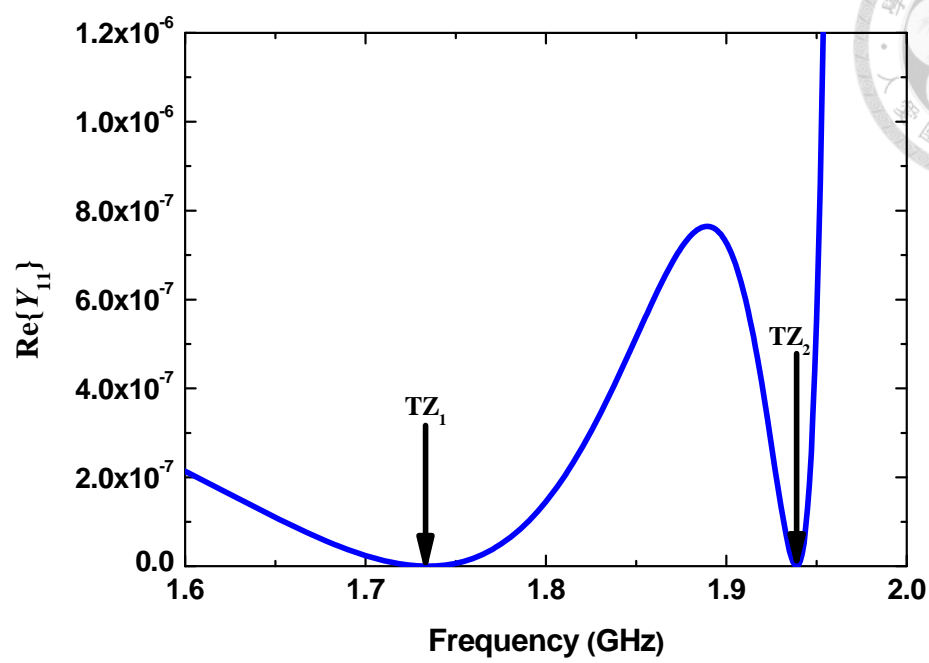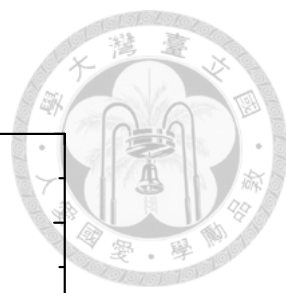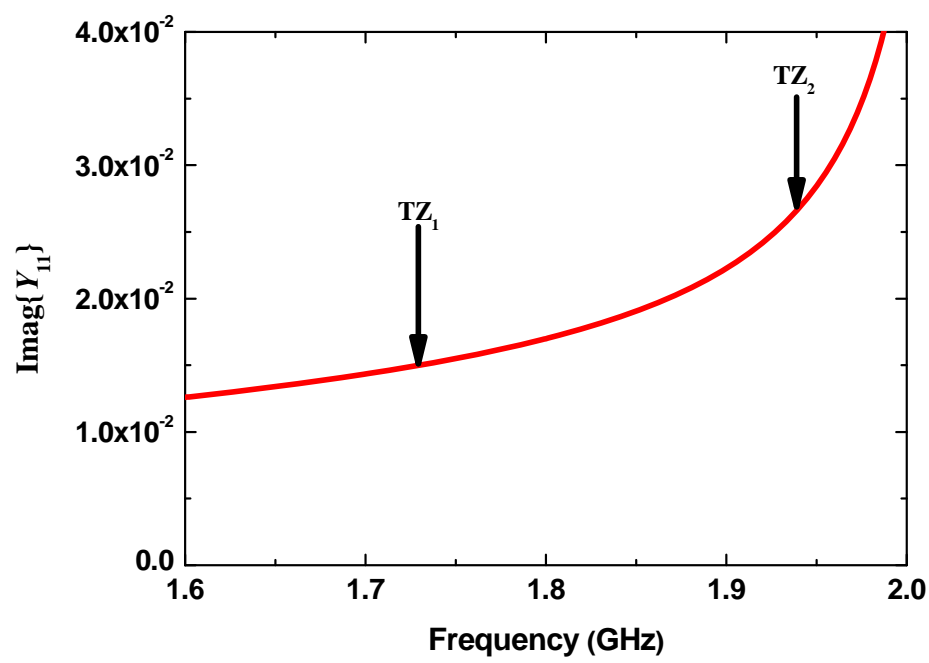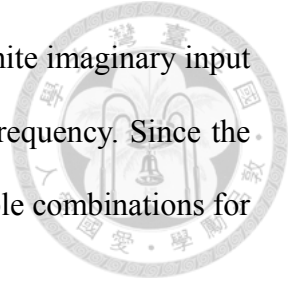Table 3.1 Combinations of loading element

	Filter 1	Filter 2
Loading element	C	C
	L	L
	L	C
	C	L

The loading elements listed in Table 3.1 are circuit components which have the same input admittance as the filters in TZ frequencies. Since the loading elements act as shunt circuit components, it is reasonable that their effects can be eliminated by adding additional shunt circuits. In the following discussion, we assume that the center frequencies of two filters are ω_1 and ω_2, respectively, and $\omega_2 > \omega_1$.

Case 1 (capacitance, capacitance)

For case 1, we define two terms

C_1 : The loading capacitance when looks into filter 1 at ω_2

C_2 : The loading capacitance when looks into filter 2 at ω_1

A shunt parallel *LC* tank can be added as the matching network, as shown in Fig. 3.3. The value of *L* and *C* should satisfy

$$\omega_1 = \frac{1}{\sqrt{L(C+C_2)}}, \tag{3.1}$$

$$\omega_2 = \frac{1}{\sqrt{L(C+C_1)}}. \tag{3.2}$$

By solving (3.1) and (3.2), *C* and *L* can be obtained as

$$C = \frac{\omega_1^2 C_2 - \omega_2^2 C_1}{\omega_2^2 - \omega_1^2}, \tag{3.3}$$

$$L = \frac{1}{\omega_1^2 (C+C_2)}. \tag{3.4}$$

Since *C* and *L* are both positive values for practical implementation, criterion exists for this matching network

$$C_2 > \frac{\omega_2^2}{\omega_1^2} C_1. \tag{3.5}$$

Fig. 3.3 Loading elements and proposed matching network of case 1

Case 2 (inductance, inductance)

For case 2, we define two terms

L_1 : The loading inductance when looks into filter 1 at ω_2

L_2 : The loading inductance when looks into filter 2 at ω_1

A shunt parallel *LC* tank can be added as the matching network, as shown in Fig. 3.4. The value of *L* and *C* should satisfy

$$\omega_1 = \frac{1}{\sqrt{(L//L_2)C}},$$
(3.6)

$$\omega_2 = \frac{1}{\sqrt{(L//L_1)C}}. \tag{3.7}$$

By solving (3.6) and (3.7), C and L can be obtained as

$$L = \frac{L_1 L_2 (\omega_2^2 - \omega_1^2)}{\omega_1^2 L_2 - \omega_2^2 L_1}, \tag{3.8}$$

$$C = \frac{1}{\omega_1^2 (L//L_2)}. \tag{3.9}$$

Since C and L are both positive values for practical implementation, criterion exists for this matching network
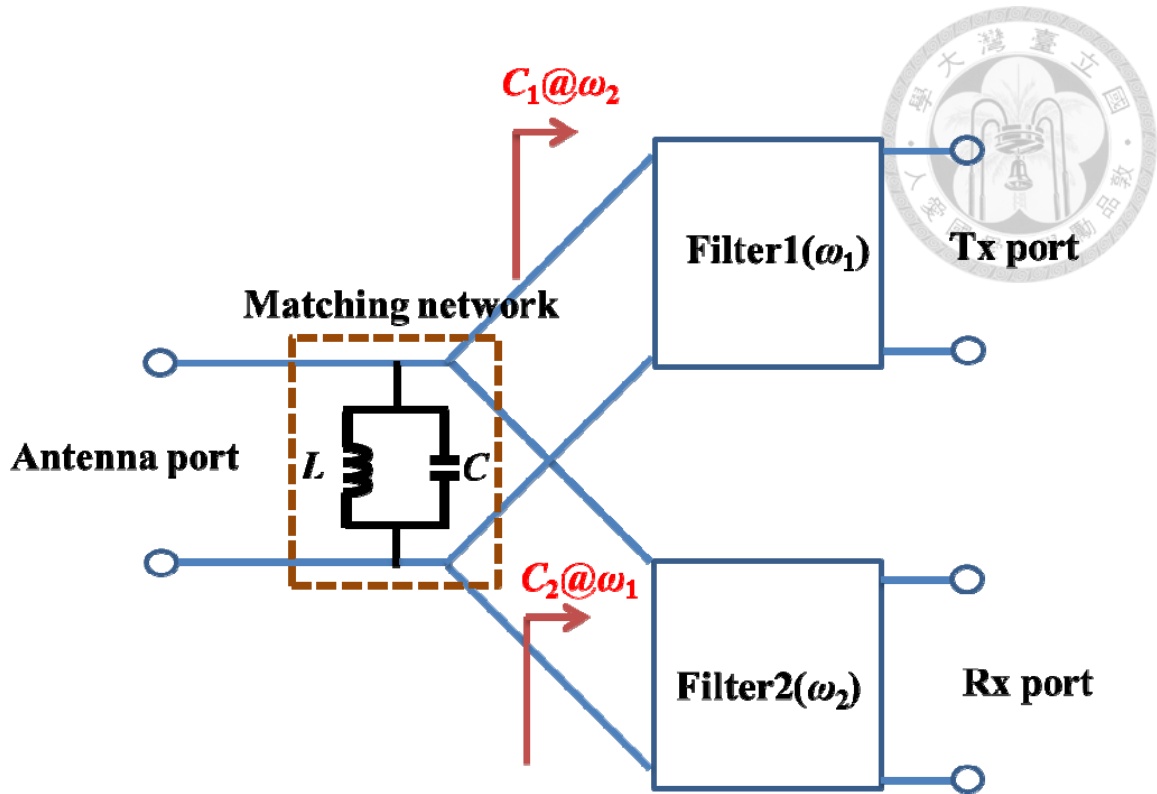
$$L_2 > \frac{\omega_2^2}{\omega_1^2} L_1. \tag{3.10}$$

37

Fig. 3.4   Loading elements and proposed matching network of case 2

Case 3 (capacitance, inductance)

For case 3, we define two terms

L_1 : The loading inductance when looks into filter 1 at ω_2

C_2 : The loading capacitance when looks into filter 2 at ω_1

A shunt parallel LC tank can be added as the matching network, as shown in Fig. 3.5.

The value of L and C should satisfy

$$\omega_1 = \frac{1}{\sqrt{L(C + C_2)}}, \qquad (3.11)$$

$$\omega_2 = \frac{1}{\sqrt{(L//L_1)C}}. \tag{3.12}$$

By solving (3.11) and (3.12), L and C can be obtained as

$$L = \frac{L_1(\omega_2^2 - \omega_1^2)}{\omega_1^2(\omega_2^2 L_1 C_2 + 1)}, \tag{3.13}$$

$$C = \frac{1}{\omega_2^2(L//L_1)}. \tag{3.14}$$

Since L and C are always positive values, no criterion exists for this matching network.
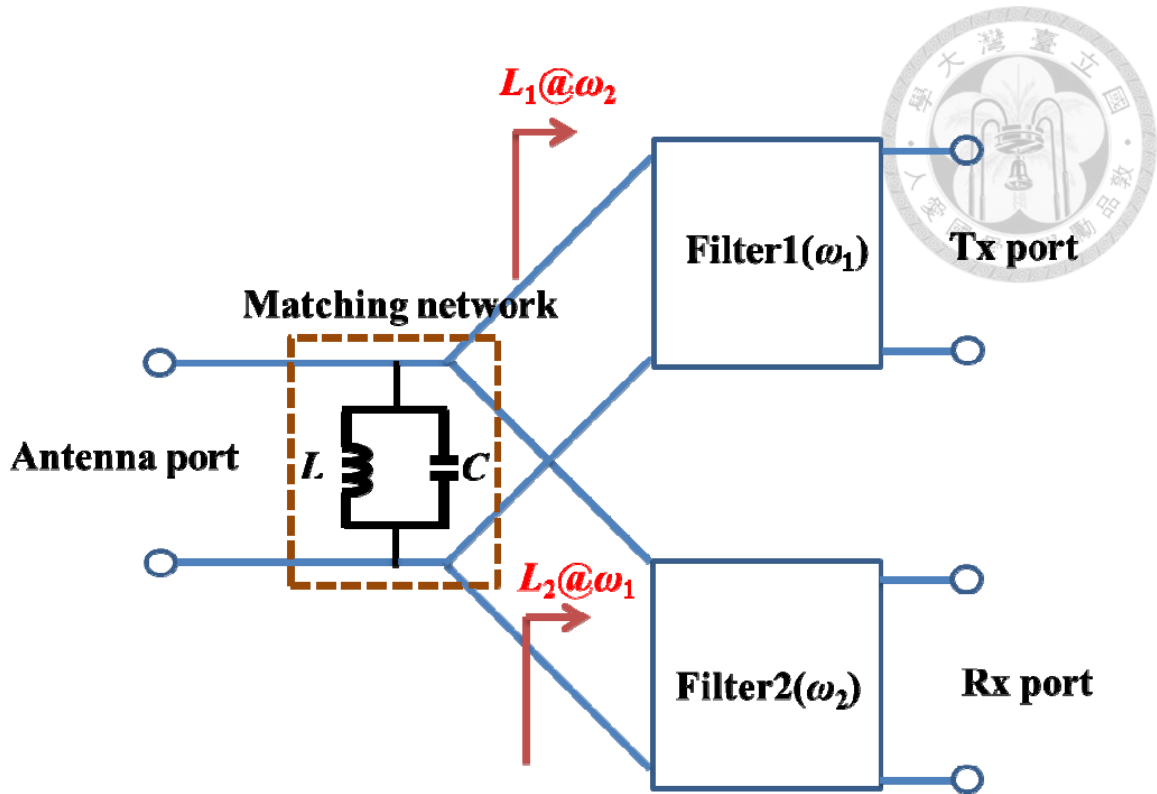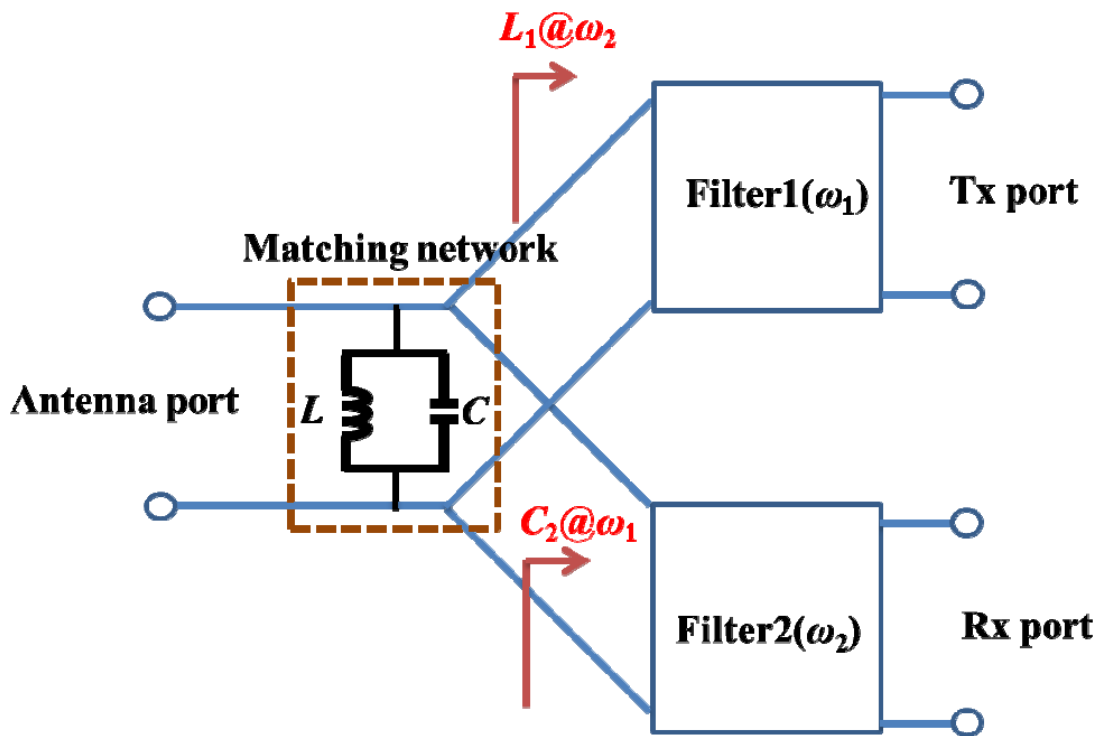

Fig. 3.5　Loading elements and proposed matching network of case 3

Case 4 (inductance, capacitance)

For case 4, we define two terms

C_1 : The loading capacitance when looks into filter 1 at ω_2

L_2 : The loading inductance when looks into filter 2 at ω_1

A shunt series *LC* tank can be added as the matching network, as shown in Fig. 3.6. The value of *L* and *C* should satisfy

$$\omega_1 = \frac{1}{\sqrt{(L+L_2)C}},\qquad(3.15)$$

$$\omega_2 = \frac{1}{\sqrt{L(C//C_1)}}.\qquad(3.16)$$

By solving (3.15) and (3.16), *C* and *L* can be obtained as

$$C = \frac{C_1(\omega_2^2 - \omega_1^2)}{\omega_1^2(\omega_2^2 L_2 C_1 + 1)},\qquad(3.17)$$

$$L = \frac{1}{\omega_2^2(C//C_1)}.\qquad(3.18)$$

Since *L* and *C* are always positive values, no criterion exists for this matching network.
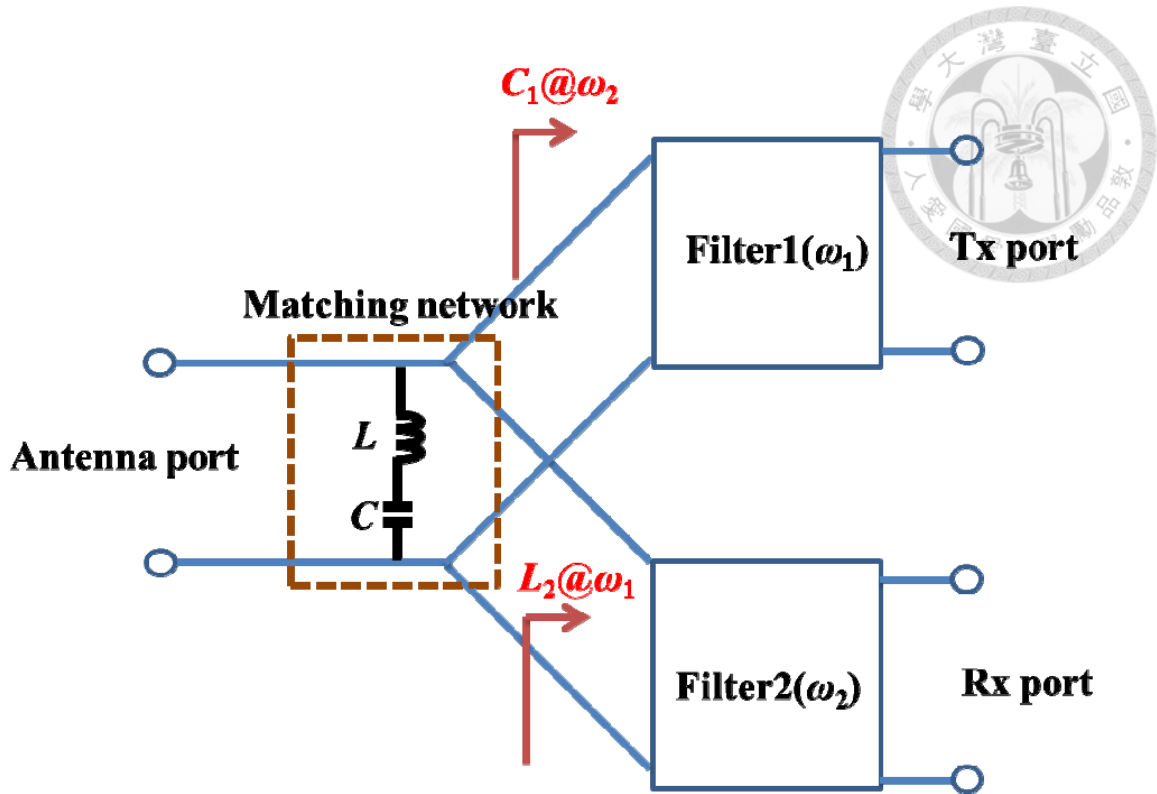
Fig. 3.6   Loading elements and proposed matching network of case 4

Based on above analysis, there are some criterions for case 1 and case 2. However, these criterions can be removed by adding more circuit elements. We will further discuss these two special cases.

Criterion 1 ($C_2 > \dfrac{\omega_2^2}{\omega_1^2} C_1$)

As shown in Fig. 3.7, if criterion 1 is not satisfied, by adding a series LC tank in front of filter 1, its input admittance can be transformed from capacitive element to inductive element without affecting the matching in passband if

$$\omega_1 = \frac{1}{\sqrt{L_s C_s}}, \tag{3.19}$$

$$\frac{1}{\sqrt{L_s(C_s // C_1)}} < \omega_2. \tag{3.20}$$

After solving (3.19) and (3.20), L_s and C_s can be obtained as

$$C_s < \frac{C_1(\omega_2^2 - \omega_1^2)}{\omega_1^2}, \tag{3.21}$$

$$L_s = \frac{1}{\omega_1^2 C_s}. \tag{3.22}$$

When the loading condition changes to case 3, the matching network for case 3 can be applied since no criterion exists for case 3.
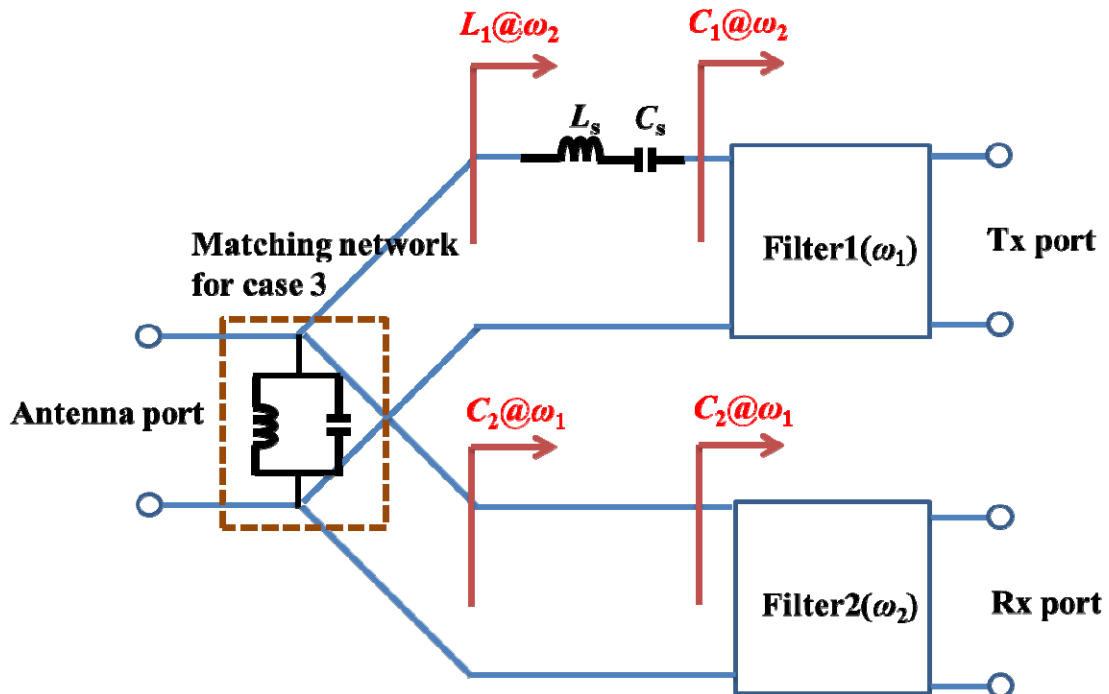

Fig. 3.7   Method for solving criterion 1
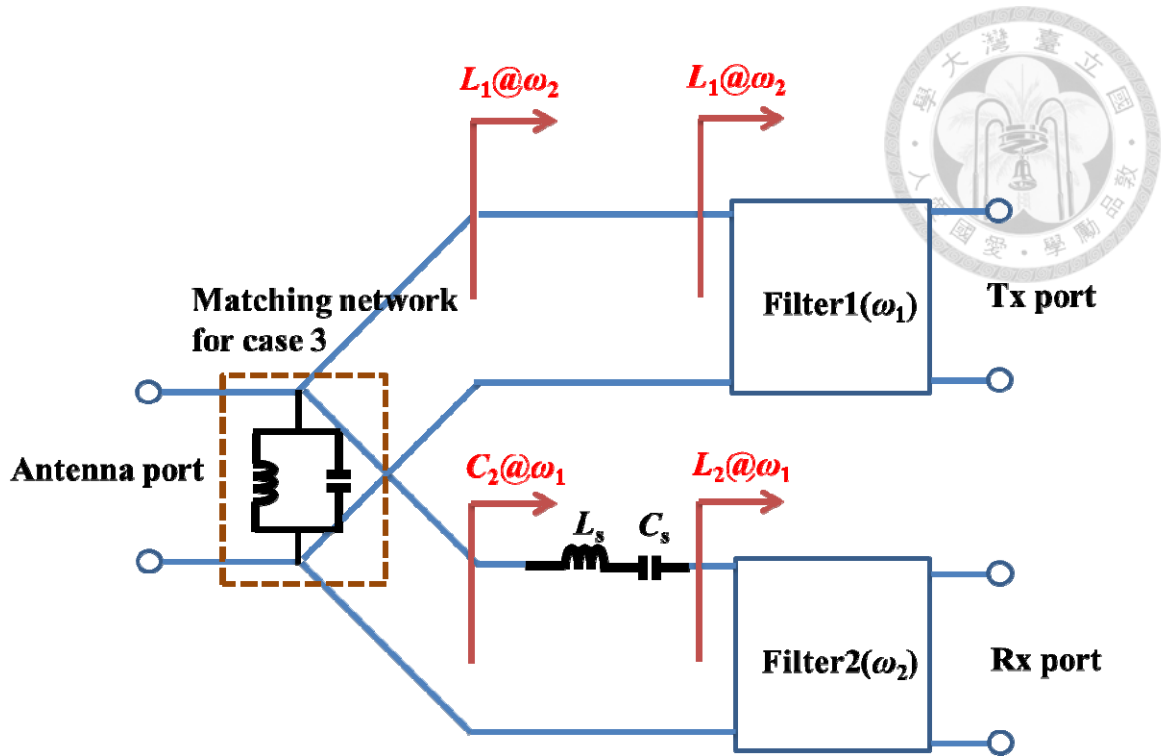
Fig. 3.8　Method for solving criterion 2

Criterion 2 ($L_2 > \dfrac{\omega_2^2}{\omega_1^2} L_1$)

As shown in Fig. 3.8, if criterion 2 is not satisfied, by adding a series LC tank in front of filter 2, its input admittance can be transformed from inductive element to capacitive element without affecting the matching in passband if

$$\omega_2 = \frac{1}{\sqrt{L_s C_s}},\qquad\qquad (3.23)$$

$$\frac{1}{\sqrt{(L_s // L_2)C_s}} > \omega_1. \qquad\qquad (3.24)$$

After solving (3.23) and (3.24), L_s and C_s can be obtained as

43

$$L_s > \frac{\omega_1^2 L_2}{\omega_2^2 - \omega_1^2},$$

(3.25)

$$C_s = \frac{1}{\omega_2^2 L_s}.$$

(3.26)

When the loading condition changes to case 3, the matching network for case 3 can be applied since no criterion exists for case 3.

Lumped Duplexer Design

A duplexer is designed for LTE band 4 application, in which Tx band is 1710~1755 MHz and Rx band is 2110~2155 MHz.

After extracting the input admittance of filter 1 and filter 2 from circuit simulation, there loading elements can be obtained as $C_1 = 0.74616 \text{ pF}$ and $C_2 = 1.3776 \text{ pF}$, which correspond to loading condition in Case 1. Therefore, the *LC* matching network can be calculated as $C = 0.48012 \text{ pF}$ and $L = 4.5402 \text{ nH}$. Fig. 3.9 shows response of the duplexer which contains two filters designed in chapter 2 and the proposed *LC* matching network. Port 1, 2, 3 are antenna port, Tx port and Rx port, respectively. Good matching can be seen in both Tx band and Rx band.
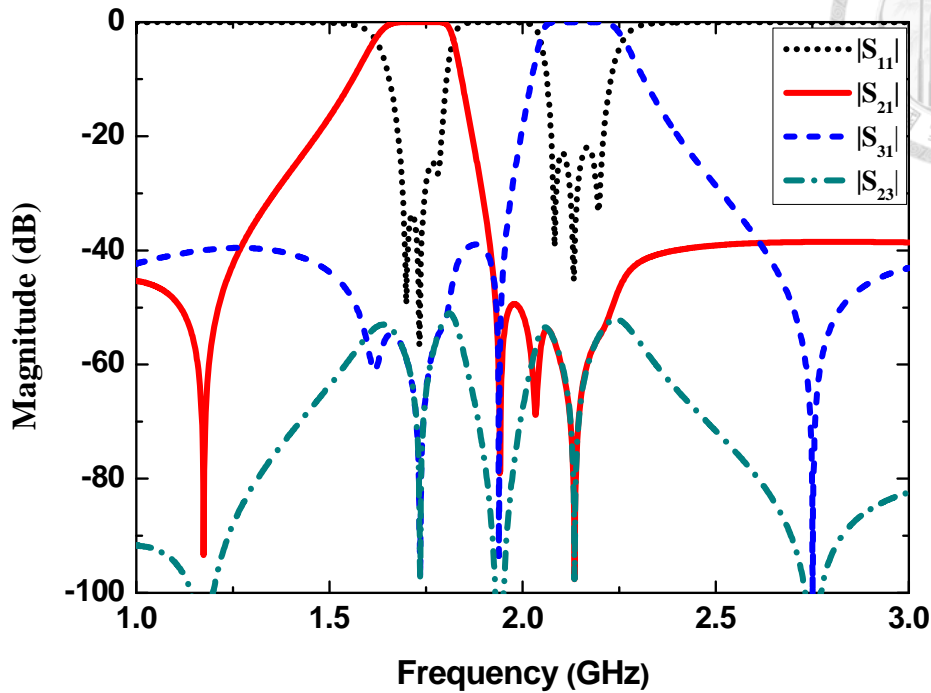
Fig. 3.9   Circuit response of the proposed duplexer

3.2   Simulation and Measurement

The lumped duplexer circuit is now implemented on LTCC substrate, which has dielectric constant 7.5 and loss tangent 0.005. The metal used in process is silver and its thickness is 13μm. The thickness of each layer is 45μm, and the number of layer is 17.

The negative shunt circuit elements can be absorbed into adjacent resonators, and the magnetic coupling between resonators can be realized by mutual inductance. Fig. 3.10 shows the circuit layout of the proposed duplexer. The excitations are designed as GSG probe platforms. The chip photo and measurement environment are shown in Fig. 3.11 and Fig. 3.12, respectively.
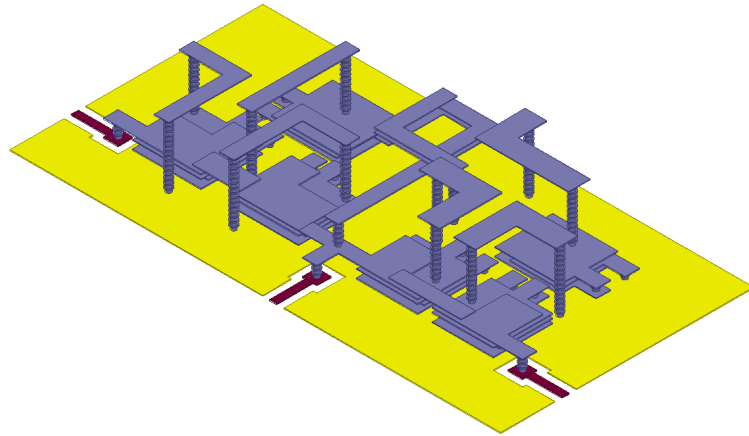
(a)
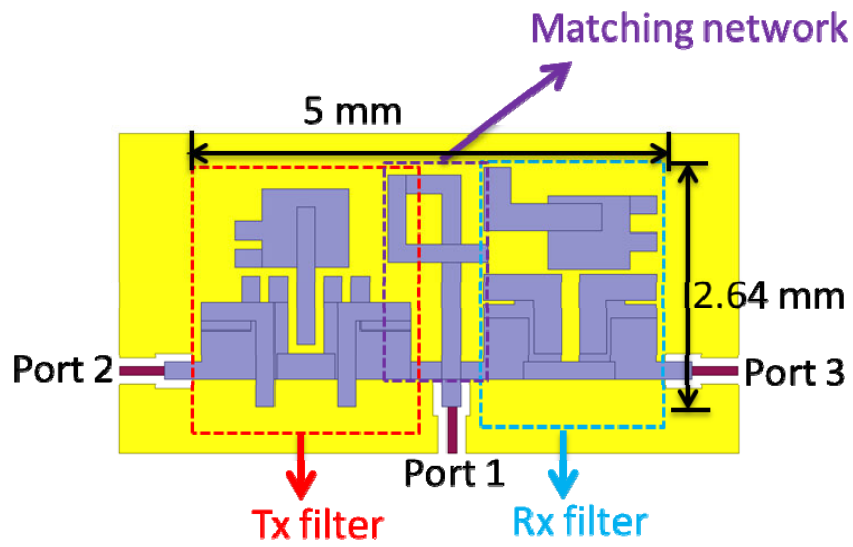
(b)
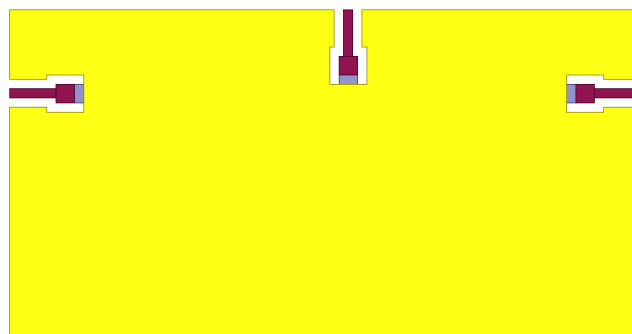
(c)

Fig. 3.10 Configuration of the proposed duplexer (a) 3D view (b) top view and (c) back view

Fig. 3.11 Chip photo

Fig. 3.12 Measurement environment

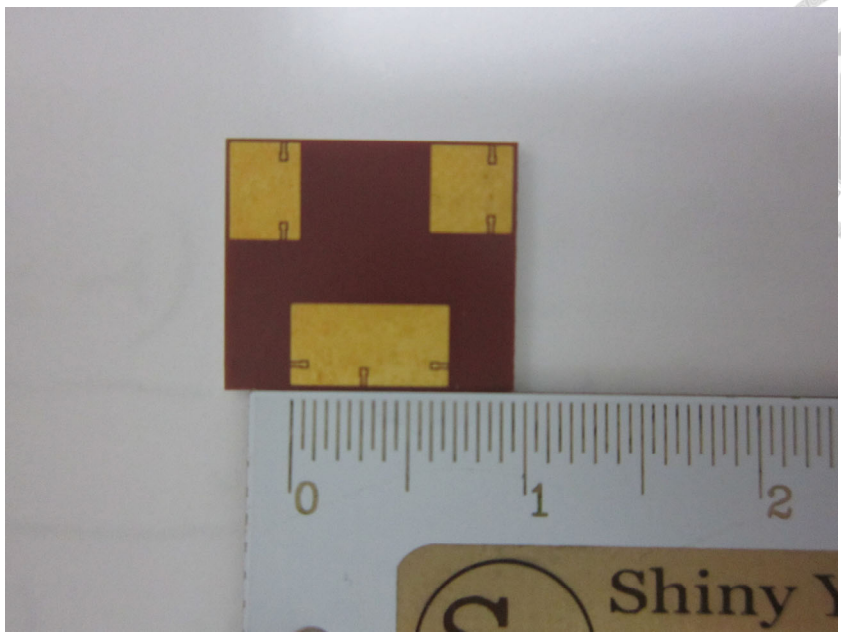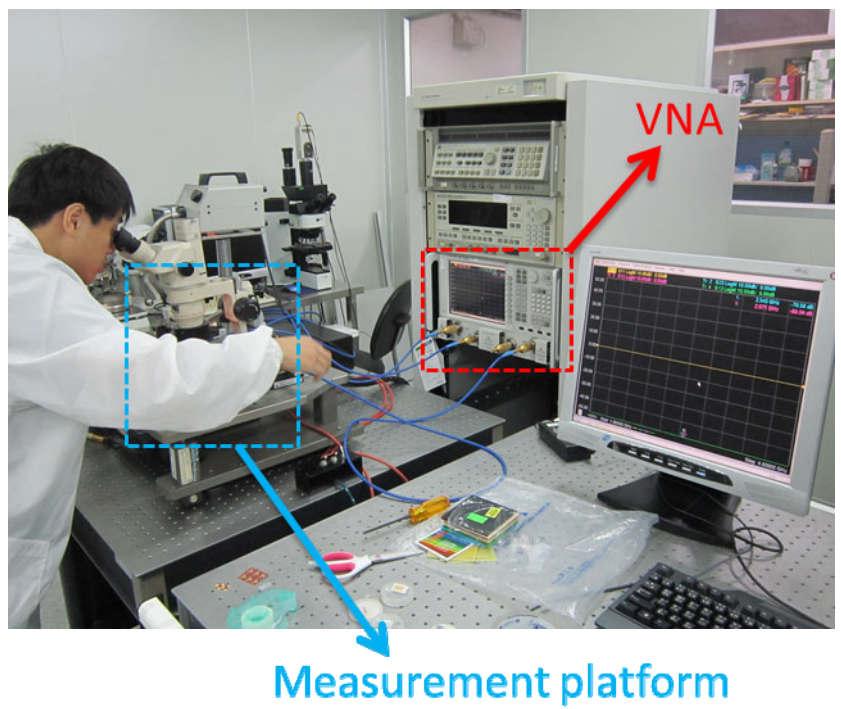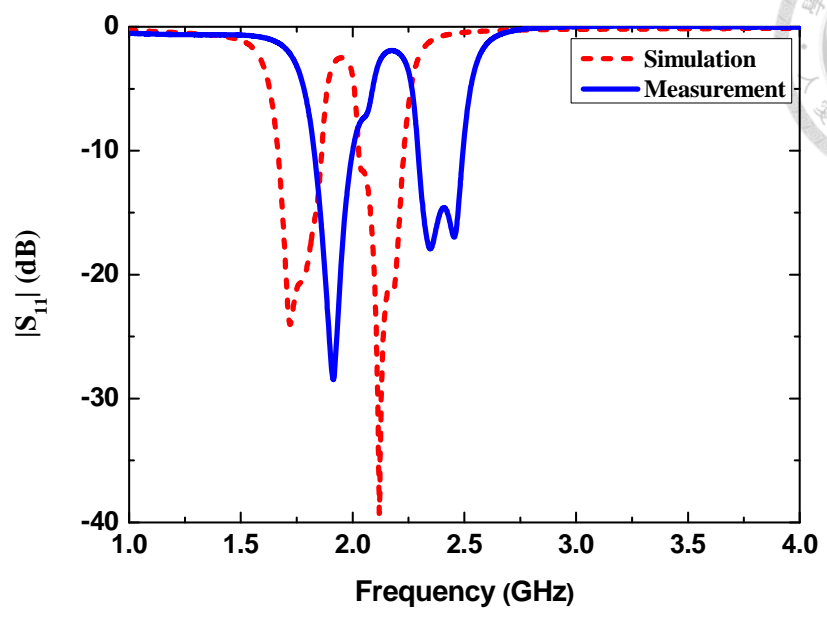The simulated and measured results are compared in Fig. 3.13 and Fig. 3.14 and listed in Table 3.2. Both Tx and Rx band responses are shifted to higher frequency, and the insertion loss is higher about 1.1 dB in measurement, which may attribute to fabrication tolerance such as change of dielectric constant and tape thickness, misalignment between layers and metal roughness issue. By adjusting dielectric constant in simulation, good agreement with measured results can be seen, as shown in Fig. 3.15. However, the matching is still satisfied. Therefore, the new frequency bands with same *FBW* are defined for performance comparison (Tx : 1872~1922 MHz, Rx : 2374~2426 MHz).

Table 3.2 Comparison between simulation and measurement (sim / mea)

	Tx-Ant	Ant-Rx
Insertion loss (dB)	2.1 / 3.2	2.4 / 3.4
Return loss (dB)	20 / 18	21 / 14
Suppression (dB)	49 / 48	
Isolation (dB)	46 / 50	
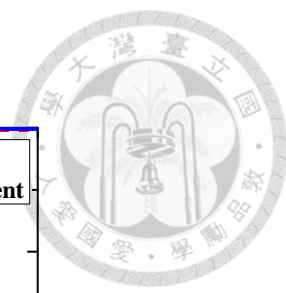
(a)
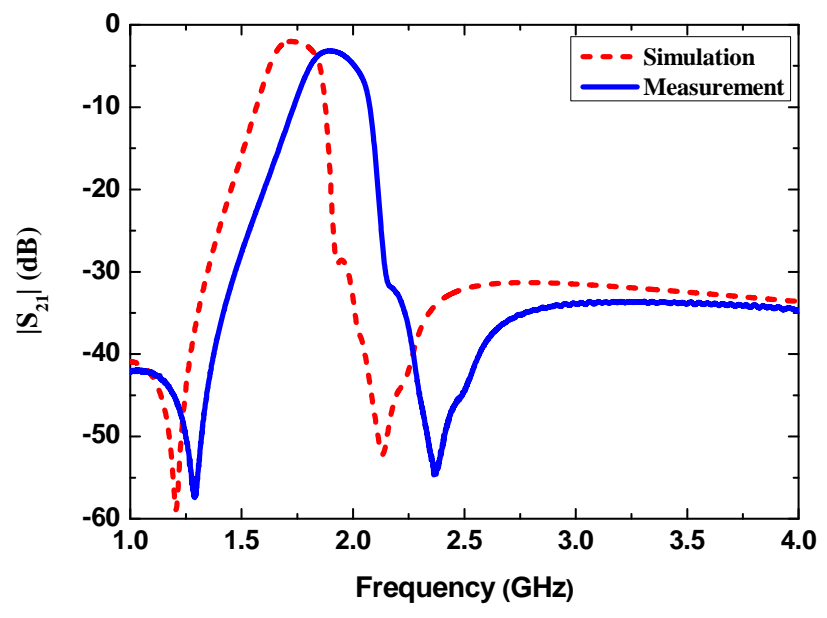
(b)

Fig. 3.13 Simulated and measured results for proposed duplexer (a) $|S_{11}|$ (matching) (b)

$|S_{21}|$ (Tx)
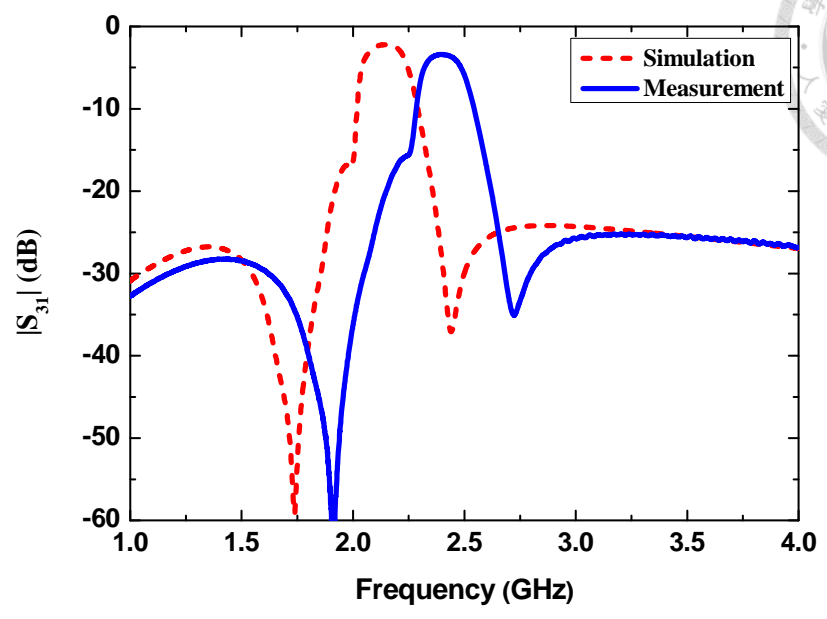
(a)
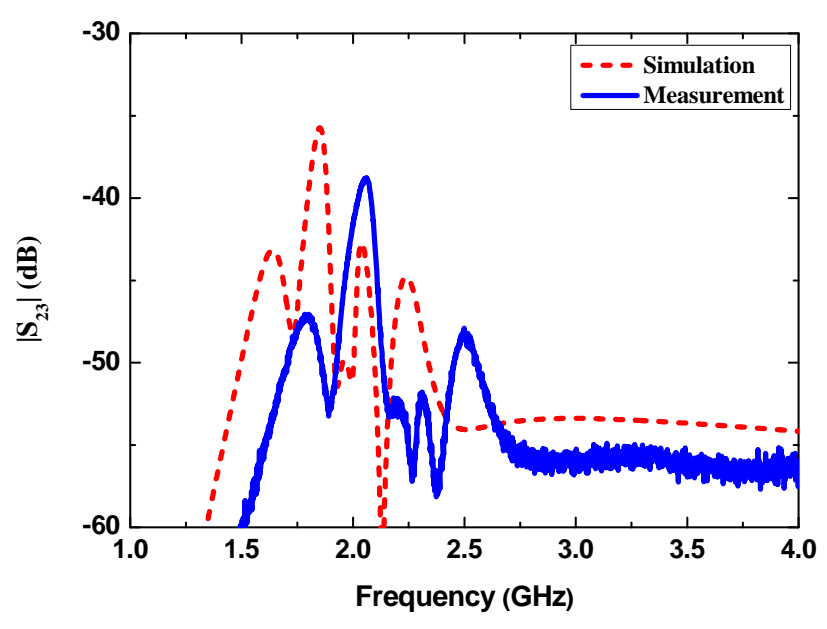
(b)

Fig. 3.14 Simulated and measured results for proposed duplexer (a) $|S_{31}|$ (Rx) (b) $|S_{23}|$

(isolation)

Fig. 3.15 Comparison between measured results and simulated results with modified dielectric constant

Table 3.3 summarizes the performance of proposed duplexer and related literature. Compared to the previous works, the proposed duplexer achieves higher isolation and suppression level in smaller area, which is suitable for modern communication system.

Comparison

Table 3.3 Performance summary and comparison of the duplexer in related literature

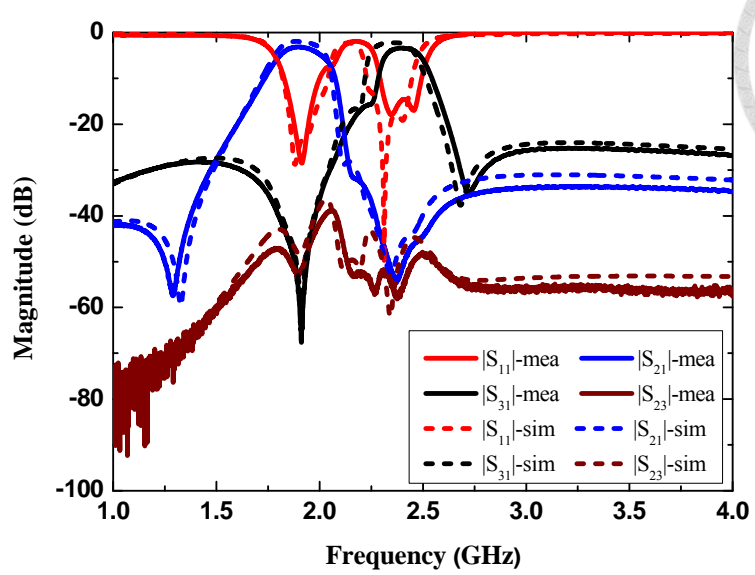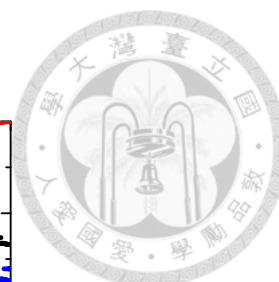| Ref	Process	Frequency (GHz)	Insertion loss (dB)	Suppression (dB)	Isolation (dB)	Size
[3]	PCB	2 / 1.6	2.1	37	37	$0.6 \times 0.32 \; \lambda_g^2$ $87.6 \times 46.5 \; mm^2$
[4]	PCB	2.4 / 1.8	2	40	40	$0.64 \times 0.19 \; \lambda_g^2$ $74.8 \times 22.7 \; mm^2$
[6]	PCB	2.45 / 1.8	2.15	25	25	$0.42 \times 0.38 \; \lambda_g^2$ $37.8 \times 34.1 \; mm^2$
[11]	PCB	2 / 1.5	2.8	40	40	$0.44 \times 0.27 \; \lambda_g^2$ $54.4 \times 33.9 \; mm^2$
[12]	PCB	2.35 / 1.75	1.44	30	28	$0.23 \times 0.12 \; \lambda_g^2$ $26 \times 14 \; mm^2$
[10]	LTCC	2.4 / 2	*3	30	30	$0.097 \times 0.037 \; \lambda_g^2$ $6.25 \times 2.5 \; mm^2$
This work	LTCC	2.4 / 1.9	3.4	48	50	$0.072 \times 0.038 \; \lambda_g^2$ $5 \times 2.64 \; mm^2$

*Estimate from figure of measured results

3.3　Summary

In this chapter, general loading effect in duplexer topology has been introduced, and new matching networks are proposed for miniaturization design. Both simulated and measured results are given and compared with previous works. Good performance can be achieved by using proposed lumped circuit topology.

Chapter 4 Duplexer for Close Separated Bands

4.1 Combination of Bandpass Filter and Diplexer

For some communication systems, the Tx and Rx frequency bands are close separated, such as LTE Band 1, which makes achieving high isolation level between two bands a challenging work. In [18], a new duplexer schematic for LTE Band 1 application is proposed, as shown in Fig. 4.1. Basically, it is the combination of bandpass filter (BPF) and diplexer. The first stage is a wide-band BPF which covers both Tx and Rx bands, while the second stage is a diplexer for separating signals of different frequency into two paths, as illustrated in Fig. 4.2. In comparison with conventional schematic based on two narrow-band bandpass filters and the matching network, all filters in [18] are wide-band filters and thus can achieve better insertion loss.
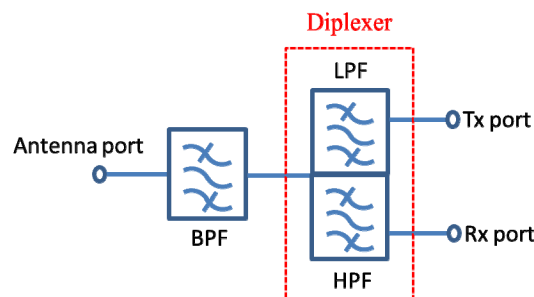

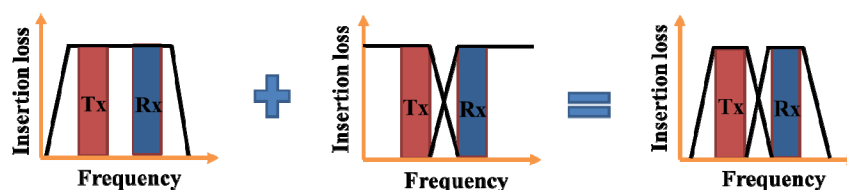Fig. 4.1   Duplexer schematic proposed in [18]

Fig. 4.2   Concept of schematic proposed in [18]

Fig. 4.3 shows the filter circuits implemented in [18], the bandpass filter is a simple two pole topology, while the low-pass filter and high-pass filter are basically third-order topologies with two TZs at each other's bands. This topology is suitable for introducing TZs at second stage for isolation enhancement, also the high input impedance resulting from resonances of parallel LC tanks can substitute the additional matching network.
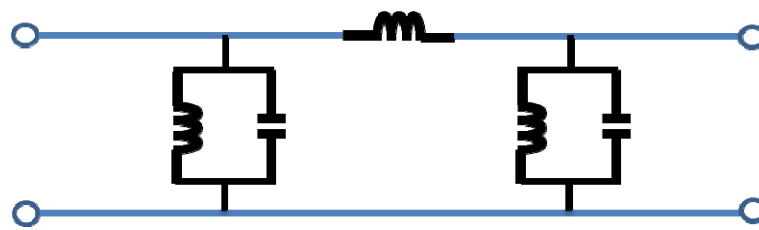
(a)
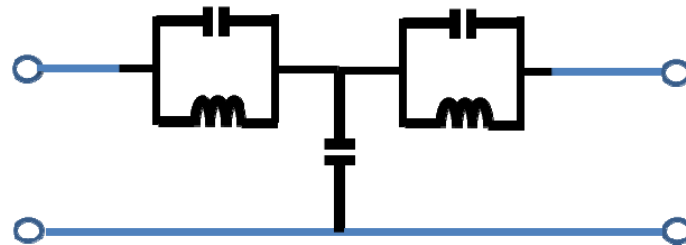
(b)
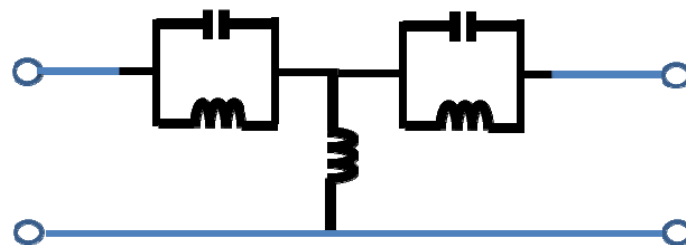
(c)

Fig. 4.3   Filter circuits used in [18] (a) bandpass filter (b) low-pass filter (c) high-pass filter

In modern systems, it is important to avoid interference between various communication applications, such as LTE, Bluetooth (2400~2484 MHz) and GPS (1570~1575 MHz). The bandpass filter shown in Fig. 4.3(a), however, cannot achieve good isolation at both Bluetooth and GPS bands due to insufficient selectivity. Besides, TZs introduced by cascading two *LC* tanks in the signal path are also inefficient for isolation improvement.

4.2   Proposed Improved Circuit Model

In this chapter, an improved circuit model for isolation enhancement is proposed for LTE Band 1 application (Tx : 1920~1980 MHz, Rx : 2110~2170 MHz), and its concept is demonstrated in Fig. 4.4. We use a selective bandpass filter to provide isolation at GPS and Bluetooth bands. Also, the second stage now contains two bandstop filters (BSFs), which can introduce three TZs result from both high-impedance path and low-impedance path, thus the isolation level can be improved efficiently.
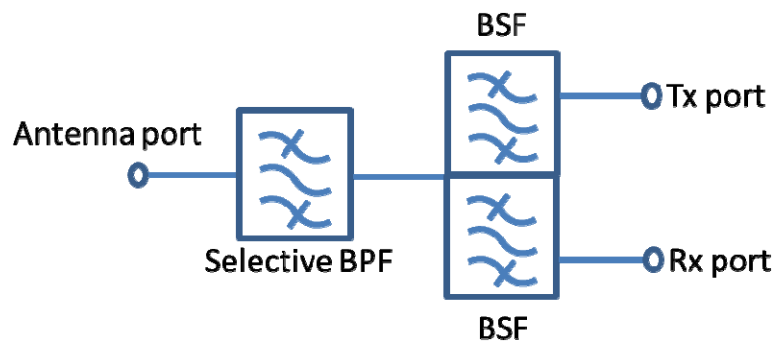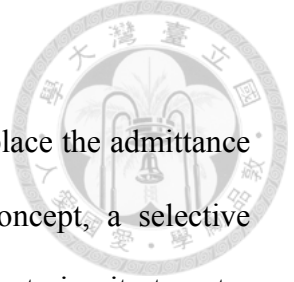

Fig. 4.4   Proposed duplexer schematic

Selective bandpass filter design

A simple method of introducing TZ at finite frequency is to replace the admittance inverter in topology by parallel *LC* tank [25]. Based on this concept, a selective bandpass filter is proposed as shown in Fig. 4.5(a), and its equivalent circuit at center frequency is shown in Fig. 4.5(b). The design procedure is described as follows.

Step 1) Design a conventional second-order Chebyshev bandpass filter to cover both Tx and Rx bands based on prototype, then convert it into lumped circuit as plotted in Fig. 4.5(b). Notice that J_{01} and J_{23} should be implemented by the inductor, and J_{12} should be implemented by capacitor.

Step 2) Replace the L_J and C_J by equivalent parallel *LC* tanks. The value of *LC* tanks can be obtained as

$$L_1 = L_J(1 - \frac{\omega_0^2}{\omega_{z1}^2}), \tag{4.1}$$

$$C_1 = \frac{1}{\omega_{z1}^2 L_1}, \tag{4.2}$$

$$L_2 = \frac{\omega_0^2 - \omega_{z2}^2}{C_J \omega_0^2 \omega_{z2}^2}, \tag{4.3}$$

$$C_2 = \frac{1}{\omega_{z2}^2 L_2}. \tag{4.4}$$

Where ω_0 is the center frequency of the bandpass filter, while ω_{z1} and ω_{z2} are specified TZs around Bluetooth and GPS bands, respectively.

Step 3) Since the equivalent circuit is valid only at center frequency, optimization is required for better matching in passband.
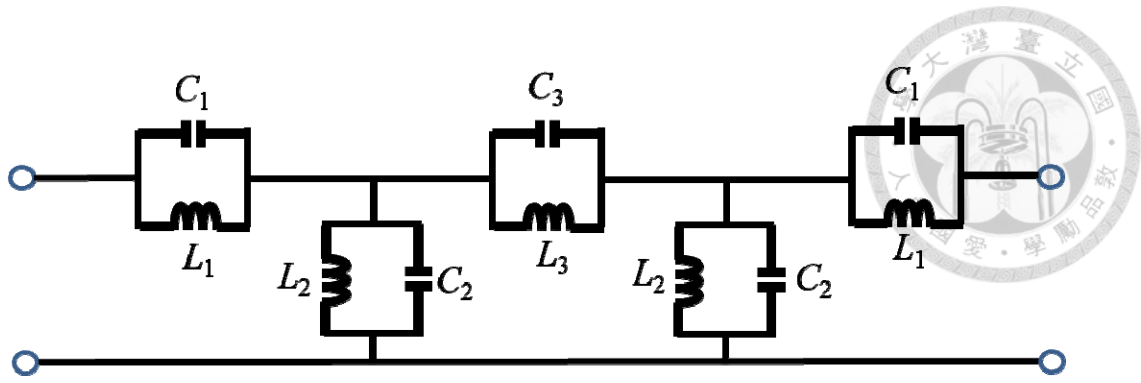
(a)
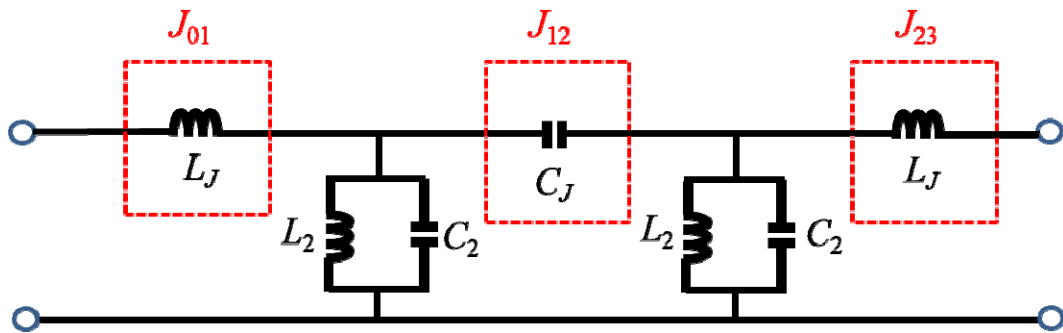
(b)

Fig. 4.5　Proposed bandpass filter (a) circuit topology (b) equivalent circuit at center frequency

Based on the design procedure, a selective bandpass filter is designed with the circuit parameters listed in Table 4.1. Fig. 4.6 shows the response of the bandpass filter.

Table 4.1 Circuit parameters of the bandpass filter

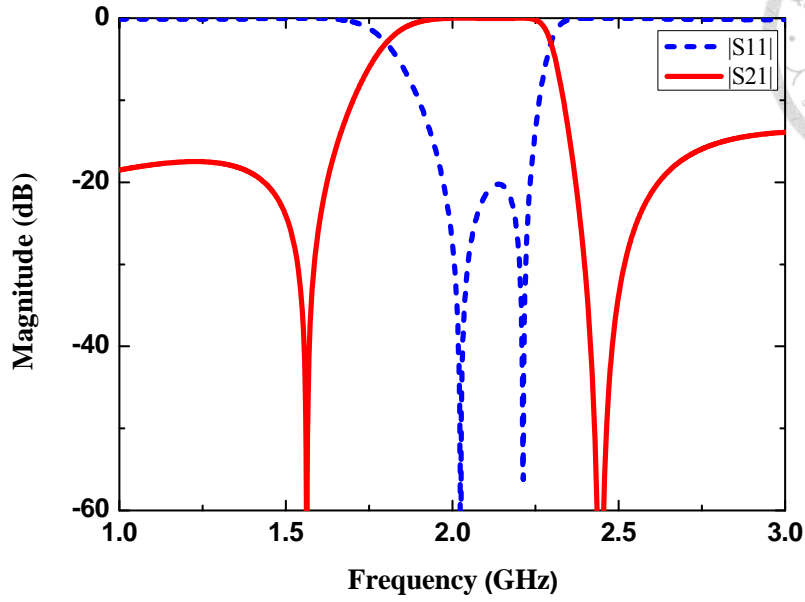| C_1 (pF)	C_2 (pF)	C_3 (pF)
5.3	3.5	3.05
L_1 (nH)	L_2 (nH)	L_3 (nH)
0.8	1.78	3.4

Fig. 4.6 Response of the selective bandpass filter

Bandstop filter design

The proposed bandstop filter topology is shown in Fig. 4.7. Isolation level can be improved since both high-impedance path and low-impedance path can be generated by parallel and series resonance. Though this goal can be achieved by using conventional third-order bandstop filter, the required circuit elements are often impractically large or small. Therefore, a higher-order circuit topology is adopted here.

To generate two TZs at desired frequencies, two equations for high-impedance path and low-impedance path are given as

$$\omega_{z1} = \frac{1}{\sqrt{L_4 C_4}}, \tag{4.5}$$

$$\omega_{z2} = \frac{1}{\sqrt{2 L_5 C_5}}. \tag{4.6}$$

58

Since the TZ is very close to passband, we can assign a reflection zero at the edge of passband to achieve better impedance matching. The even and odd mode analysis can be applied due to symmetry of the schematic. The condition for generating a reflection zero at ω_p is given as

$$Y_{even} * Y_{odd} = Y_0^2, \tag{4.7}$$

Where

$$Y_{even} = \cfrac{j}{\cfrac{\omega_p L_4}{\omega_p^2 L_4 C_4 - 1} + \cfrac{2\omega_p L_5}{\omega_p^2 L_5 C_5 - 1} + \cfrac{2}{\omega_p^2 C_5}}, \tag{4.8}$$

$$Y_{odd} = \frac{j(\omega_p^2 L_4 C_4 - 1)}{2\omega_p L_4}. \tag{4.9}$$

After assigning a suitable value for C_4, the rest circuit elements can be obtained as

$$L_5 = \frac{\omega_p^2 - 2\omega_{z2}^2}{4B\omega_p\omega_{z2}^2}, \tag{4.10}$$

$$B = \frac{-Y_0^2(A+D)}{A+Y_0^2}, \tag{4.11}$$

$$A = \frac{C_4(\omega_p^2 - \omega_{z1}^2)}{\omega_p}, \tag{4.12}$$

$$D = \frac{C_4(\omega_p^2 - \omega_{z1}^2)(\omega_p^2 - 2\omega_{z2}^2)}{\omega_p^3}, \tag{4.13}$$

$$L_4 = \frac{1}{\omega_{z1}^2 C_4},$$
(4.14)

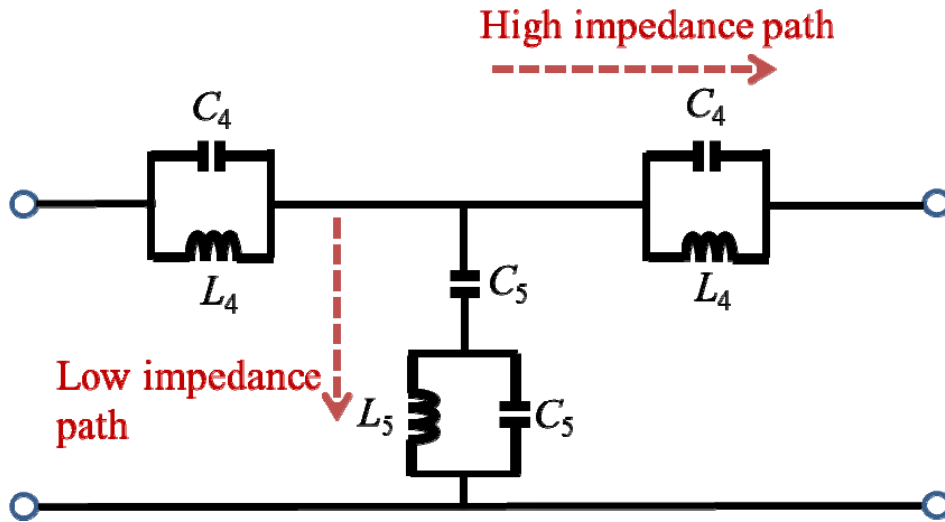$$C_5 = \frac{1}{2\omega_{z2}^2 L_5}.$$
(4.15)

Fig. 4.7 Proposed bandstop filter topology

Two bandstop filters are designed for Tx and Rx. In consideration of insertion loss, TZs are distributed around stopband. The circuit parameters are listed in Table 4.2 and their responses are shown in Fig. 4.8.

Table 4.2 Circuit parameters of bandstop filters

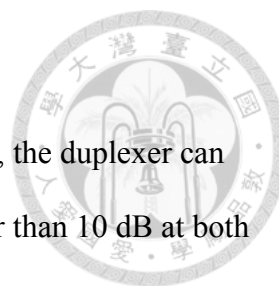| Filter 1 (Tx)			Filter 2 (Rx)		
ω_p	ω_{z1}	ω_{z2}	ω_p	ω_{z1}	ω_{z2}
1.98 GHz	2.13 GHz	2.31 GHz	2.11 GHz	1.96 GHz	1.83 GHz
C_4 (pF)		C_5 (pF)	C_4 (pF)		C_5 (pF)
7		0.629	7		1.343
L_4 (nH)		L_5 (nH)	L_4 (nH)		L_5 (nH)
0.798		3.776	0.942		2.817
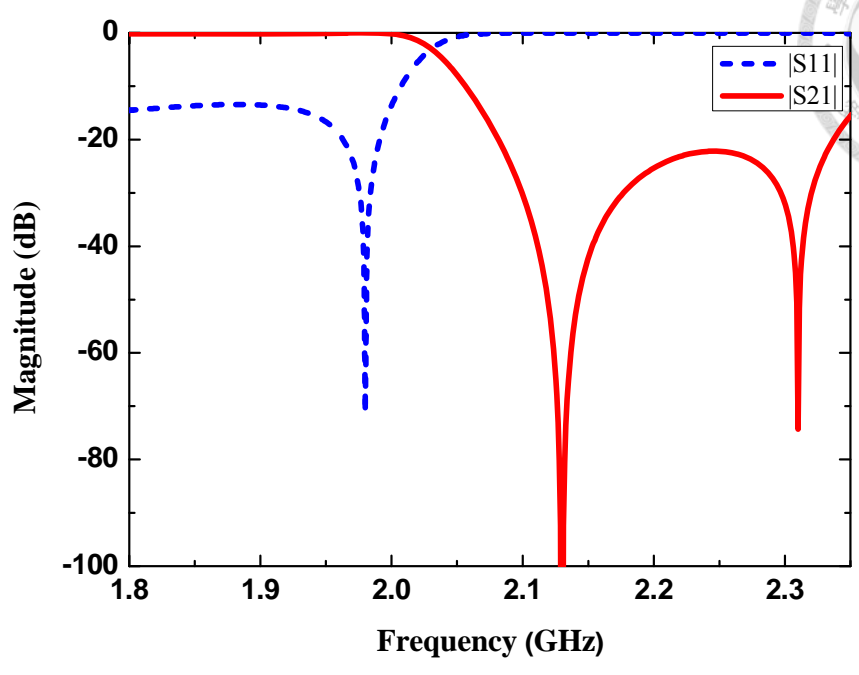
(a)
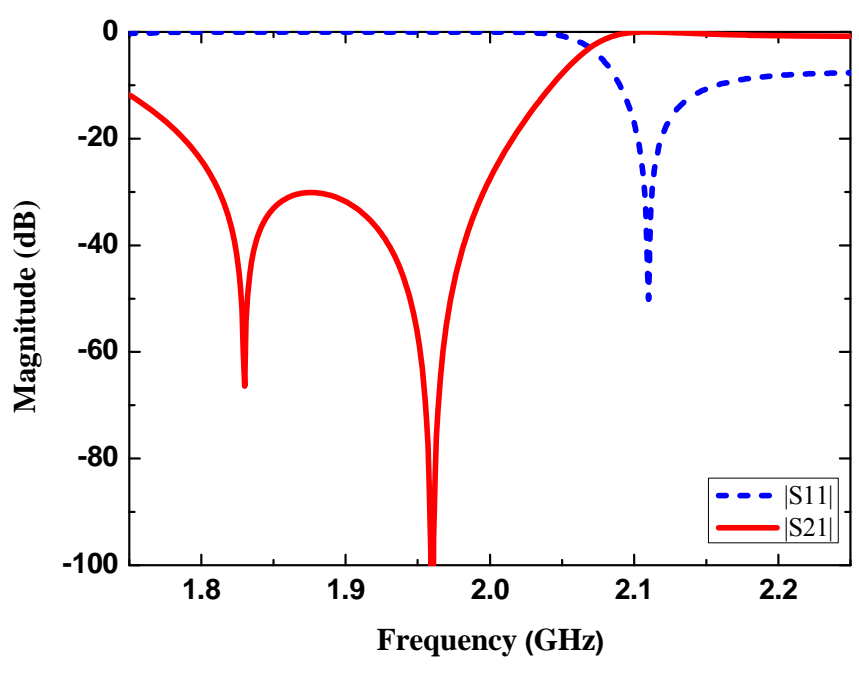
(b)

Fig. 4.8　Response of bandstop filters (a) filter 1 (Tx) (b) filter 2 (Rx)

61

Duplexer schematic

After designing bandpass filter and bandstop filters individually, the duplexer can be constructed, and its response is shown in Fig. 4.9. The S_{11} is better than 10 dB at both Tx and Rx bands, and all TZs can be predicted accurately.
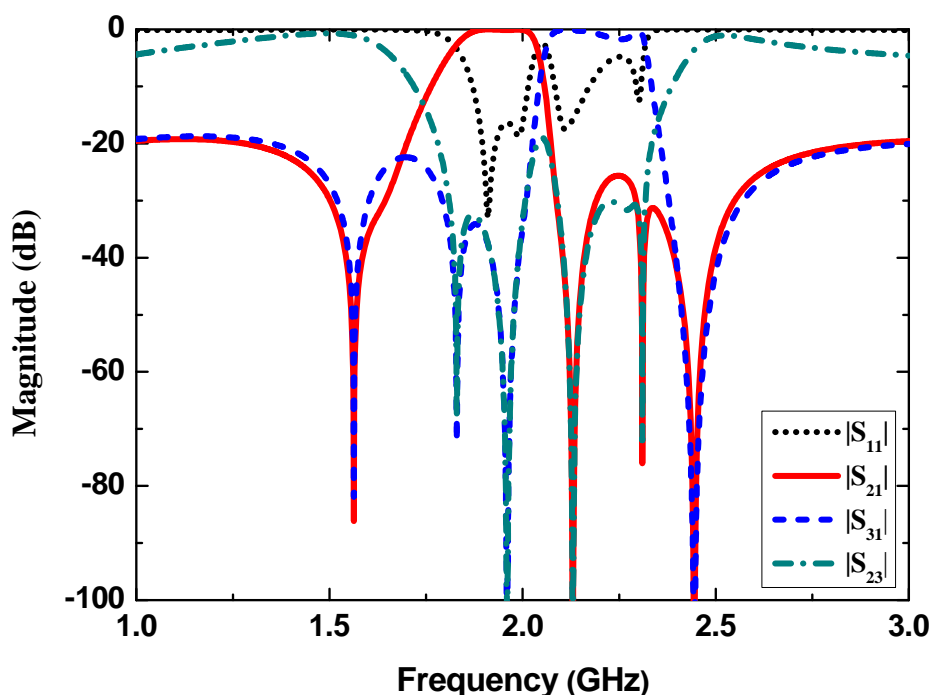
Fig. 4.9   Circuit response of the proposed duplexer

4.3   Simulation and Measurement

The lumped duplexer circuit is now implemented on LTCC substrate, which has dielectric constant 7.5 and loss tangent 0.005. The metal used in process is silver and its thickness is 13μm. The thickness of each layer is 45μm, and the number of layer is 17.

Fig. 4.10 and Fig. 4.11 show the circuit layout and chip photo of the proposed duplexer, respectively. The excitations are designed as GSG probe platforms. The

simulated and measured results are compared in Fig. 4.12 and Fig. 4.13, Both Tx and Rx responses are shifted to higher frequency in measurement. Unfortunately, the matching in Rx band is not well as prediction, which may attribute to fabrication tolerance such as change of dielectric constant, tape thickness and misalignment between layers, thus affects the insertion loss of Rx band.
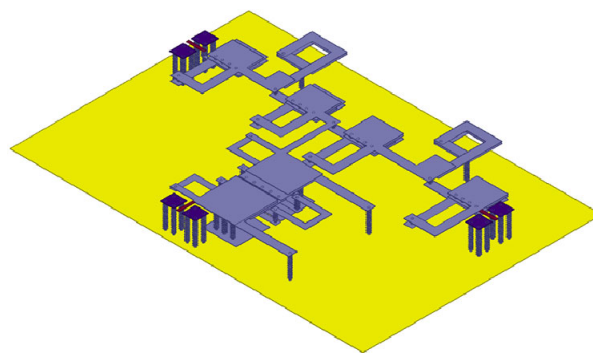
(a)
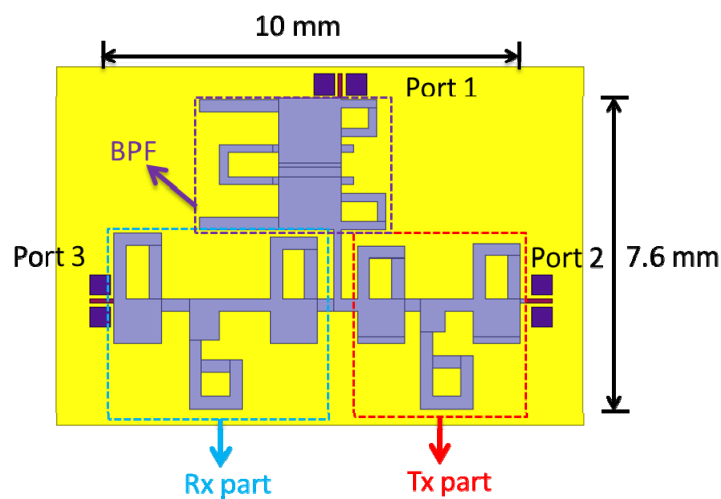
(b)

Fig. 4.10 Configuration of the proposed duplexer (a) 3D view (b) top view
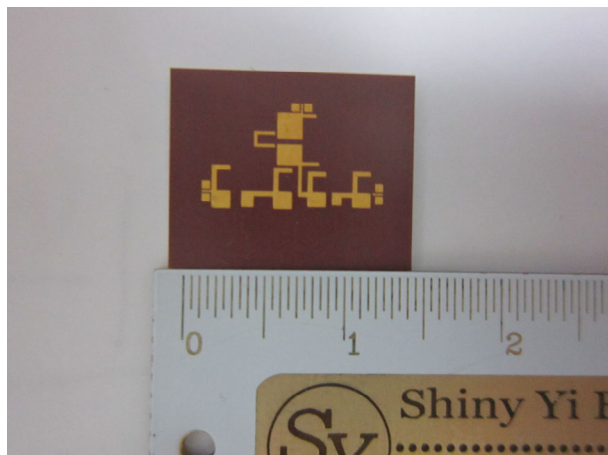
Fig. 4.11 Chip photo

However, the stopband can still be observed from measured results, therefore new frequency bands are defined for performance comparison (Tx：1942~2002 MHz, Rx：2153~2213 MHz). The ratio of two defined bands is close to specification of LTE Band 1. Table 4.3 summarizes the performance of proposed duplexer with previous work in [18]. In comparison with [18], this work achieves higher isolation level between Tx and Rx bands, also the suppression at GPS and Bluetooth bands are improved.
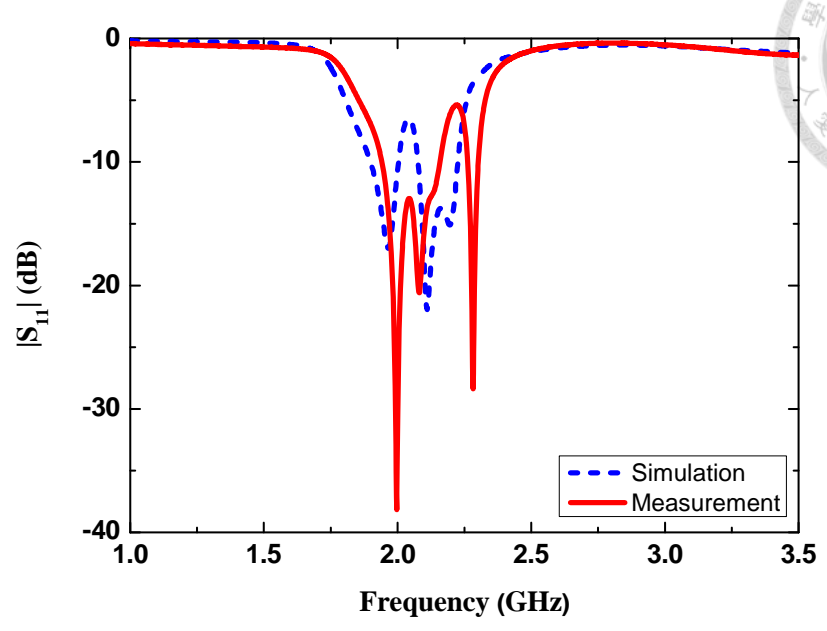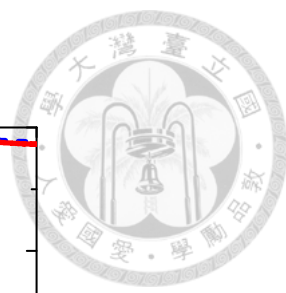
(a)
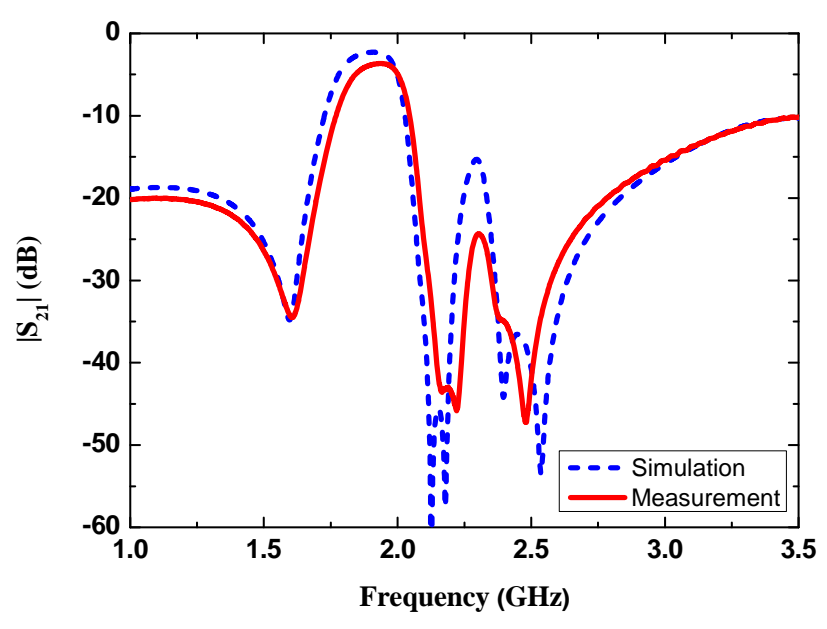
(b)

Fig. 4.12 Simulated and measured results for proposed duplexer (a) $|S_{11}|$ (matching) (b) $|S_{21}|$ (Tx)
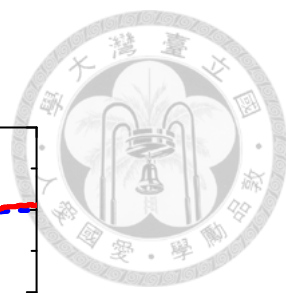
(a)
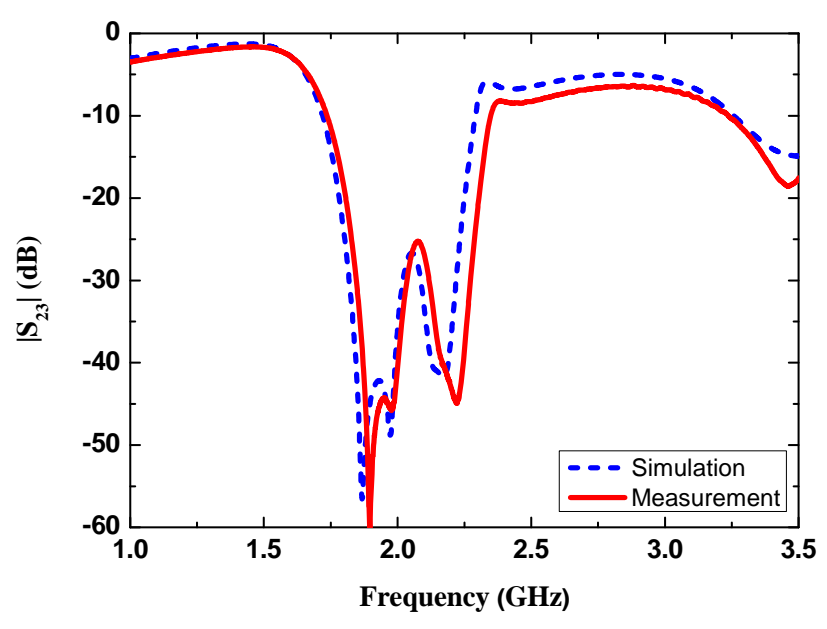
(b)

Fig. 4.13 Simulated and measured results for proposed duplexer (a) $|S_{31}|$ (Rx) (b) $|S_{23}|$

(isolation)

Table 4.3 Performance summary and comparison

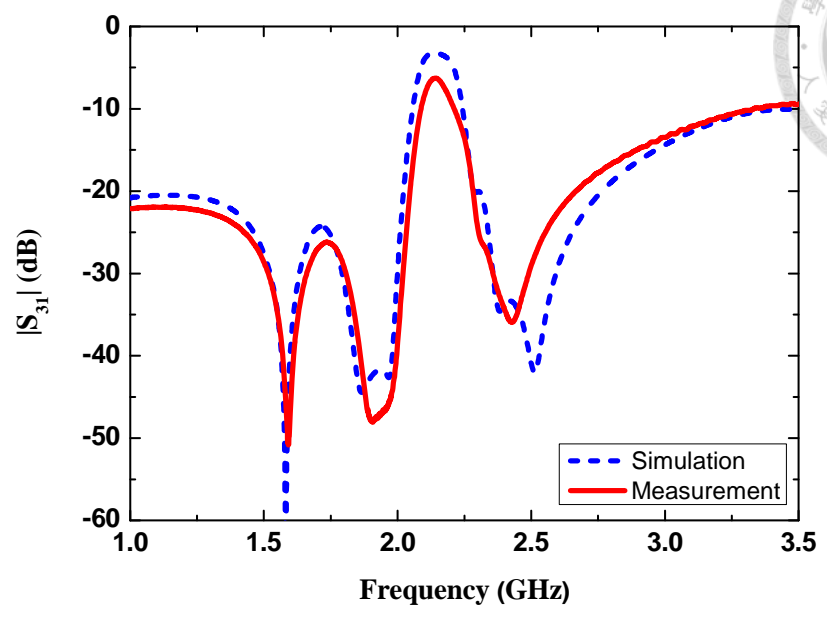| Ref	Process/Layer	Insertion loss (dB)	Suppression at Tx & Rx (dB)	Isolation (dB)	Suppression at GPS/Bluetooth (dB)	Size
[18]	LTCC/30	4.5	30	30	12/15	3x2.5x1.2 mm^3
This work	LTCC/17	6.4	38	38	31/30	10x7.6x0.9 mm^3

4.4 Summary

In this chapter, a schematic for two close bands is proposed and analyzed. Both simulated and measured results are given and compared with previous work. The isolation level at Tx and Rx bands can be further improved by introducing both high-impedance path and low-impedance path. Also, the suppression at GPS/Bluetooth bands are enhanced due to additional TZs.

Chapter 5   Conclusions
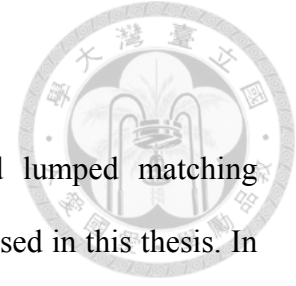
Based on the theory of cross-coupled bandpass filter and lumped matching networks, a miniaturized duplexer with high isolation level is proposed in this thesis. In addition, a duplexer schematic suitable for two close bands is also proposed and analyzed.

In chapter 3, the design methodology for a miniaturized duplexer is proposed. By analyzing different combination of loading elements, conventional T-junction or dual-mode resonator can be replaced by lumped matching circuit, thus the circuit size can be significantly miniaturized. The size of the proposed duplexer is $0.072 \times 0.038 \, \lambda_g^2$. In addition, the isolation level is high compared with several previous works. The minimum isolation is 50 dB.

In chapter 4, the design methodology for a lumped duplexer is proposed. By introducing high-impedance path and low-impedance path, isolation level can be improved even for two close separated bands. Also 30 dB suppression is achieved at GPS/Bluetooth bands by using the selective bandpass filter. The minimum isolation is 38 dB.

References

[1]   3GPP website : http://www.3gpp.org/.

[2]   J.-W Sheen, "LTCC-MLC Duplexer for DCS-1800," *IEEE Trans. Microwave Theory Tech.*, vol. 47, pp. 1883–1890, September 1999.

[3]   T. Ohno, K. Wada, and O. Hashimoto, "Design Methodologies of Planar Duplexers and Triplexers by Manipulating Attenuation Poles," *IEEE Trans. Microwave Theory Tech.*, vol. 53, pp. 2088–2095, June 2005.

[4]   F. Cheng, X.-Q. Lin, Z.-B. Zhu, L.-Y. Wang and Y. Fan, "High isolation diplexer using quarter-wavelength resonator filter," *Electron. Lett.*, vol. 48, pp. 330–331, Mar. 2012.

[5]   E. E. Djoumessi, "Compact packaged Diplexer Based on Highly Selective Dual-Mode Bandpass Filter," in *IEEE Microwave Magazine.,* vol. 12, pp. 89–93, Feb. 2011.

[6]   H.-W Liu, W.-Y. Xu, Z.-C. Zhang, and X.-H. Guan, "Compact Diplexer Using Slotline Stepped Impedance Resonator," *IEEE Microwave Wireless Comp. Lett.*, vol. 23, pp. 75–77, Feb. 2013.

[7]   C.-H. Tseng and H.-J. Chen, "Signal-interference Stepped-impedance-Line Microstrip Filters and Application to Duplexers," *IEEE Microwave Wireless Comp. Lett.*, vol. 21, pp. 421–423, Aug. 2011.

[8]   A. F. Sheta, J. P. Coupez, G. Tanne, and S. Toutain, "Miniature microstrip stepped impedance resonator bandpass filters and diplexers for mobile communications," in *IEEE MTT-S Int. Microwave Symp*. Dig., 1996, pp. 607–610.

[9]   C.-M. Tsai, S.-Y. Lee, C.-C. Chuang, and C.-C. Tsai, "A folded coupled-line structure and its application to filter and diplexer design," in *IEEE MTT-S Int.*

Microwave Symp. Dig., 2002, pp. 1927–1930.

[10] C.-W. Tang, and S.-F. You, "Design Methodologies of LTCC Bandpass Filters, Diplexer, and Triplexer With Transmission Zeros," *IEEE Trans. Microwave Theory Tech.*, vol. 54, pp. 717–723, Feb. 2006.

[11] C.-F. Chen, T.-Y. Huang, C.-P. Chou, and R.-B. Wu, "Microstrip Diplexers Design With Common Resonator Sections for Compact Size, But High Isolation," *IEEE Trans. Microwave Theory Tech.*, vol. 54, pp. 1945–1952, May 2006.

[12] T. Yang, P.-L. Chi, and T. Itoh, "Compact Quarter-Wave Resonator and Its Applications to Miniaturized Diplexer and Triplexer," *IEEE Trans. Microwave Theory Tech.*, vol. 59, pp. 260–269, Feb. 2011.

[13] T. Yang, and G. M. Rebeiz, "Three-Pole 1.3–2.4-GHz Diplexer and 1.1–2.45-GHz Dual-Band Filter With Common Resonator Topology and Flexible Tuning Capabilities," *IEEE Trans. Microwave Theory Tech.*, vol. 61, pp. 3613–3624, Oct. 2013.

[14] J.-Y. Zou, C.-H. Wu, and T.-G. Ma, "Miniaturized diplexer using synthesized microstrip lines with series LC tanks," *IEEE Microwave Wireless Comp. Lett.*, vol. 22, pp. 354–356, July. 2012.

[15] M. Fritz and W. Wiesbeck, "A Diplexer Based on Transmission Lines, Implemented in LTCC," *IEEE Trans. Microwave Theory Tech.*, vol. 29, pp. 427–432, Aug. 2006.

[16] K.-H. Li, C.-W. Wang, and C.-F. Yang, "A Miniaturized Diplexer Using Planar Artificial Transmission Lines for GSM/DCS Applications," in *Proc. Asia Pacific Microwave Conf.*, 2007, pp. 1–4.

[17] C.-H. Lai, G.-T. Zhou, and T.-G. Ma, "On-Chip Miniaturized Diplexer Using Jointed Dual-Mode Right-/Left-Handed Synthesized Coplanar Waveguides on

GIPD Process," *IEEE Microwave Wireless Comp. Lett.*, vol. 24, pp. 245–247, Apr. 2014.

[18] J.-Y Lee, S.-W. Choi, and K.-B. Lee, "Development of 2GHz Band Micro LTCC Duplexer by Combining BPF and Diplexer," in *Proc. Asia Pacific Microwave Conf.*, 2011, pp. 1047–1050.

[19] R. J. Cameron, R. Mansour, and C. M. Kudsia, *Microwave Filters for Communication Systems : Fundamentals, Design and Applications*. New York: Wiley, 2007.

[20] S. Amari, "Direct Synthesis of Folded Symmetric Resonator Filters with Source-Load Coupling," *IEEE Microwave Wireless Comp. Lett.*, vol. 11, pp. 264–266, June. 2001.

[21] D. M. Pozar, *Microwave Engineering*. 4th ed. New York: Wiley, 2001.

[22] J.-S Hong, *Microstrip Filters for RF / Microwave Applications*. 2nd ed. New York: Wiley, 2011.

[23] C.-W. Tang, "Design of four-ordered cross-coupled bandpass filters with low-temperature co-fired ceramic technology," *IET Micro. Antennas Propag.*, vol. 3, pp. 402–409, 2009.

[24] G. Matthaei, E.M.T. Jones, L. Young, *Microwave Filters, Impedance-Matching Networks, and Coupling Structures*. London: Artech House, 1980.

[25] R. Levy, and P. Petre, "Design of CT and CQ Filters Using Approximation and Optimization," *IEEE Trans. Microwave Theory Tech.*, vol. 49, pp. 2350-2356, Dec. 2001.